2019

# Design of an ultra-wideband microstrip antenna array with low size, weight and power

Paul Staffan
*Wright State University*

# DESIGN OF AN ULTRA-WIDEBAND MICROSTRIP ANTENNA ARRAY WITH LOW SIZE, WEIGHT AND POWER

A thesis submitted in partial fulfillment of the requirements
for the degree of Master of Science in Electrical Engineering

By

PAUL STAFFAN
B.S.E.E., Wright State University, 1993

2019
Wright State University

WRIGHT STATE UNIVERSITY

GRADUATE SCHOOL

**Decemeber 9, 2019**

I HEREBY RECOMMEND THAT THE THESIS PREPARED UNDER MY SUPERVISION BY Paul Staffan ENTITLED Design of an ultra-wideband Microstrip Antenna Array with Low Size, Weight and Power BE ACCEPTED IN PARTIAL FULFILLMENT OF THE REQUIREMENTS FOR THE DEGREE OF Master of Science in Electrical Engineering

Michael A. Saville, Ph.D., PE
Thesis Director

Fred Garber, Ph.D. Interim Chair,
Department of Electrical Engineering

Committee on Final Examination:

Yan Zhuang, Ph.D.

Saiyu Ren, Ph.D.

Josh Ash, Ph.D.

Barry Milligan, Ph.D.
Interim Dean of the Graduate School

## ABSTRACT

Staffan, Paul. MSEE, Electrical Engineering, Wright State University, 2019. Design of an ultra-wideband Microstrip Antenna Array with Low Size, Weight and Power.

This study focuses on the use of microstrip antenna technology for designing an ultra-wideband antenna to meet low size, weight and power requirements. Based on the recent literature for such antennas, a quasi-log periodic microstrip antenna array is designed to operate from 8 to 40 GHz (radar bands X, Ku, K and Ka). The array consists of 33 co-linear, inset-fed, square patches on a Roger's Duroid substrate, and is modeled using the Advanced Design System software from Keysight. The simulated results show the antenna has pass-band gains greater than 5 dB, a half-power beamwidth of 30 degrees, and linear polarization with a broadside radiation pattern. In addition, the fractional voltage standing wave ratio is less than 1.8 for 18 GHz of the pass-band, and the antenna has an efficiency greater than 60 percent over the entire pass band.

# TABLE OF CONTENTS


**1 Introduction** **1**

1.1 Motivation . . . . . 1

1.2 Challenges . . . . . 2

1.3 Hypothesis . . . . . 3

1.4 Outline of Thesis . . . . . 4

**2 Background** **4**

2.1 Log Periodic Antenna Design . . . . . 4

2.2 Patch Antenna Design . . . . . 6

2.2.1 Design . . . . . 6

2.2.2 BW Enhancement Techniques . . . . . 8

2.2.3 Feeding Methods . . . . . 10

2.2.4 Voltage and Current Distribution . . . . . 11

2.2.5 Input Impedance . . . . . 14

2.2.6 Radiation Pattern . . . . . 16

2.2.7 Transmission Line Design Method . . . . . 18

2.2.8 Effective Permittivity . . . . . 18

2.2.9 Fringing Effect . . . . . 19

2.2.10 Resonant Frequency . . . . . 19

2.2.11 Feed Line Length . . . . . 20

2.2.12 Modes, Polarization, Efficiency, Gain, Pattern, Directivity . . . . . 22

2.2.13 Test and Analysis of Results . . . . . 25

2.3 Technical Challenges . . . . . 26

2.3.1 Antenna Design Challenges . . . . . 26

2.3.2 Modeling and Simulation . . . . . 28

2.4 Summary . . . . . 29

**3 Methodology** **30**

3.1 How to study the problem . . . . . 30

3.2 Describe the experiment . . . . . 32

3.3 Analysis Method . . . . . 33

3.4 Evaluation of the Results . . . . . 33

3.5 Summary . . . . . 35

**4 LPMSAA Design and Simulation Results** **35**

4.1 Engineered Drawing . . . . . 35

4.2 ADS Simulation Sweeps . . . . . 35

4.3 Return Loss, VSWR, Input Impedance . . . . . 37

4.4 Far Field Data . . . . . 37

4.4.1 Half Power Beamwidth . . . . . 37

4.4.2 Electric and Magnetic Phasor Data . . . . . 42

4.4.3 Gain, Directivity and Efficiency . . . . . 42

4.4.4 Co and Cross pol Isolation . . . . . 52

4.4.5 Antenna Polarization . . . . . 52

4.5 Summary . . . . . 58

**5 Conclusions** **58**

5.1 Summary of The Results . . . . . 58

5.2 Compare LPMSAA to a Pasternack Standard Gain Horn Antenna . . . . . 59

5.3 Potential Issues . . . . . 60

5.4 Suggested Test Methods . . . . . 61

5.5 Recommendations for Future Work . . . . . 63

**Appendix A** **64**

**Appendix B** **71**

**References** **76**

# LIST OF FIGURES


1 Sketch of RMSA on large ground plane. . . . . 7

2 Tuncated patch antenna with H and U slots. . . . . 10

3 Simulated voltage and current distribution on patch antenna. . . . . 12

4 Microstrip patch antenna with inset depth, $y_0$. . . . . 13

5 Radiating slot apertures and equivalent circuit of slot conductance. . . . . 15

6 Direction of wave propagation, normal to patch. . . . . 16

7 3D, Square patch antenna simulation . . . . . 17

8 Spherical coordinate system . . . . . 18

9 Microstrip patch antenna showing fringing effect . . . . . 20

10 Partial drawing of collinear array. . . . . 21

11 Drawing depicting gain and directivity . . . . . 23

12 ADS stack-up of FR-4 for patch antenna array. . . . . 26

13 EM layout of 9-element, 2-3GHz LPMSAA, created in ADS. . . . . 30

14 Return loss simulation results for 9-element, 2-3 GHz LPMSAA. . . . . 31

15 VSWR simulation results for 9-element, 2-3 GHz LPMSAA. . . . . 32

16 Engineered drawing of LPMSAA. . . . . 36

17 8-40 GHz LPMSAA Return Loss Magnitude. . . . . 38

18 8-20 GHz LPMSAA VSWR. . . . . 38

19 20-30 GHz LPMSAA VSWR. . . . . 39

20 30-40 GHz LPMSAA VSWR. . . . . 39

21 LPMSAA, 8-20 GHz input impedance versus frequency. . . . . 40

22 LPMSAA, 20-30 GHz input impedance versus frequency. . . . . 40

23 LPMSAA, 30-40 GHz input impedance versus frequency. . . . . 41

24 10 GHz XZ plane far-field radiation intensity. . . . . 43

25 10 GHz XZ plane electric and magnetic far-field patterns. . . . . 43

26 10 GHz YZ plane far-field radiation intensity. . . . . 44

27 10 GHz YZ plane electric and magnetic far-field patterns. . . . . 44
28 20 GHz XZ plane far-field radiation intensity. . . . . 45
29 20 GHz XZ plane electric and magnetic far-field patterns. . . . . 45
30 20 GHz YZ plane far-field radiation intensity. . . . . 46
31 20 GHz YZ plane electric and magnetic far-field patterns. . . . . 46
32 30 GHz XZ plane far-field radiation intensity. . . . . 47
33 30 GHz XZ plane electric and magnetic far-field patterns. . . . . 47
34 30 GHz YZ plane far-field radiation intensity. . . . . 48
35 30 GHz YZ plane electric and magnetic far-field patterns. . . . . 48
36 40 GHz XZ plane far-field radiation intensity. . . . . 49
37 40 GHz XZ plane electric and magnetic far-field patterns. . . . . 49
38 40 GHz YZ plane far-field radiation intensity. . . . . 50
39 40 GHz YZ plane electric and magnetic far-field patterns. . . . . 50
40 8-20 GHz gain and directivity versus frequency. . . . . 51
41 20-30 GHz gain and directivity versus frequency. . . . . 51
42 30-40 GHz gain and directivity versus frequency. . . . . 51
43 LPMSAA, 10 GHz, XZ plane, $\vec{E}$ co versus cross pol. . . . . 53
44 LPMSAA, 10 GHz, YZ plane, $\vec{E}$ co versus cross pol. . . . . 53
45 LPMSAA, 20 GHz, XZ plane, $\vec{E}$ co versus cross pol. . . . . 54
46 LPMSAA, 20 GHz, YZ plane, $\vec{E}$ co versus cross pol. . . . . 54
47 LPMSAA, 30 GHz, XZ plane, $\vec{E}$ co versus cross pol. . . . . 55
48 LPMSAA, 30 GHz, YZ plane, $\vec{E}$ co versus cross pol. . . . . 55
49 LPMSAA, 40 GHz, XZ plane, $\vec{E}$ co versus cross pol. . . . . 56
50 LPMSAA, 40 GHz, YZ plane, $\vec{E}$ co versus cross pol. . . . . 56
51 10 GHz, antenna parameters screen shot. . . . . 57
52 Initial $W$, $L$ calculations. . . . . 64
53 Conductance equations. . . . . 65

54 $R_{in}$ and $Z_0$ equations. . . . . 65
55 Main transmission line equations. . . . . 66
56 Array scaling equations. . . . . 67
57 Fringing effect equations. . . . . 68
58 Starting frequency and $R_{in}$ equations. . . . . 69
59 $d_m$ and main transmission line equations. . . . . 70
60 ADS screen shot of 50 Ohm feed transmission line. . . . . 71
61 ADS screen shot 8 and 8.4 GHz patches. . . . . 72
62 ADS screen shot 8 and 8.4 GHz patches in layout view. . . . . 73
63 ADS screen shot of stack up. . . . . 73
64 ADS screen shot of frequency sweep setup window. . . . . 74
65 ADS screen shot of port settings. . . . . 74
66 ADS screen shot of mesh settings. . . . . 75

# LIST OF TABLES


1 Standard Radar Frequency Letter Band Nomenclature . . . . . 3

2 2-3 GHz LPMSAA primary parameters. . . . . 31

3 8-40 GHz LPMSAA primary parameters. . . . . 34

4 8-40 GHz LPMSAA radar band performance. . . . . 37

5 LPMSAA half-power beamwidth. . . . . 41

6 Far-field electric and magnetic field phasor data. . . . . 42

7 LPMSAA gain, directivity, and efficiency data. . . . . 42

8 Average $\vec{E}$ co to cross polarization data. . . . . 52

9 LPMSAA polarization data. . . . . 58

10 Ka band horn versus LPMSAA antenna comparison . . . . . 60

This thesis is dedicated to my wife and children who were so supportive during the research process.

# 1 Introduction

The Sensors and Signals Exploitation Lab (SSEL) at Wright State University (WSU) is a dynamic hands-on, laboratory environment for electromagnetic experimentation and development by engineering students. Students can experiment with the laboratory equipment to create radar images of target objects. The laboratory consists of an antenna positioning fixture, 4-port analyzer (43.5 GHz), and horn antennas. Students can do laboratory level experiments. Students are also encouraged to be creative and make improvements, or to optimize previous designs of hardware, or software. The motivation is to create an open learning environment where students can get experience with the "real world" of engineering, electromagnetics, and radar systems. For example, the above mentioned antenna positioning system was created by the students of the university. The students use Matlab, Comsol Multi-Physics, and ADS software for experimentation. These software programs are used to simulate and accurately depict final designs and analysis of wave propagation and radar cross-section studies [1].

## 1.1 Motivation

The lab can utilize one to four small UWB horn antennas to meet the needs of the experiment. The current horn antenna(s), singular or array can be removed or added, but it is undesirable to have to change the mechanical fixture to add or subtract horn antennas for various experiments. The typical bandwidth required for a complete system is in the range of 8-40 GHz. The laboratory is seeking a new antenna system that has a low "SWaP", size, weight, and power requirement. The proposed antenna system must also satisfy the bandwidth, gain, radiation pattern, VSWR and budget of the lab. Since microstrip antennas (MSAs) could possibly meet many of the above requirements, it is logical to seek a solution using an MSA or Microstrip Antenna Array, (MSSA).

## 1.2 Challenges

The MSA was invented by G. A. Deschamps in 1953. However, serious development did not begin for another 20 years by R.E Munson and J. Q. Howell [2]. For many reasons, MSAs have become increasingly popular in recent years. A few reasons are: they have a small-form factor, low profile, light weight, conformable, and can be wrapped around objects such as missiles or within smart phones. MSAs can be either linear or circularly polarized. They can be made compact for use in small electronic devices, and can be etched onto a circuit board. MSAs also allow for dual, triple and more frequency operations. MSAs are economical to fabricate, are relatively simple to design and simulate. With advances in simulation, feed networks, substrate technology, and a strong desire of consumers for consistently smaller, faster and lightweight electronics; it is no surprise that MSAs are becoming increasingly more popular [2–5].

Prior to a discussion of the MSA and its application to the SSEL, we need to also consider the challenges associated with MSAs. The MSAs biggest drawback is the extremely narrow bandwidth ($BW$). Albeit, with it's small footprint, so comes a narrow $BW$. Other disadvantages are low gain and power [2]. A typical single MSA patch could have a menial $BW$ of 7-10$\%$, whereas an array of 17 elements could have a $BW$ of 98$\%$ [6]. A Microstrip Antenna Array (MSAA) can be designed also for other purposes, i.e. to be more directive or to produce a high-gain pattern, etc. For our purposes, wide bandwidth is highly desirable.

With the above points in mind, it seems logical to consider the development of a MSAA to replace the horn antennas in the SSEL. There are various types of MSAAs that have been developed previously. But none have been found in research to have the ability to span such a large $BW$, and that meet our low SWaP, broadside pattern requirement. Many papers and articles focus on antennas in the sub-10 GHz bands or specific high-frequency bands, but with limited $BW$. A microstrip dipole antenna typically has a relatively large $BW$, but with an end-fire pattern which would be somewhat cumbersome in the SSEL [7, 8]. Other array

Table 1: Standard Radar Frequency Letter Band Nomenclature, (IEEE Standard 521-2002), (source: https://www.microwaves101.com/encyclopedias/frequency-letter-bands).

| Band Designator | Frequency (GHz) |
|---|---|
| X band | 8 to 12 |
| Ku band | 12 to 18 |
| K band | 18 to 27 |
| Ka band | 24 to 40 |

types considered which are popular and well-cited are UWB antennas. UWB antennas are typically used for the 3.1-10.6 GHz band. The Log Periodic Microstrip Antenna design could possibly be frequency independent, that is, can be shifted upwardly to meet our needs at the lab [4, p. 619]. Also, the Log Periodic Technique has been found to reach very wide bandwidths [9]. Many research articles still focus on 10 GHz and below for this topology but there is the potential to use the LPMSAA for higher frequencies and $BW$. Fractal antennas offer even more miniaturization and/or equivalent $BW$ capabilities but with a smaller form factor. Fractals are antennas with repeating patterns embedded in the patch to create more capacitance and inductance. Although a fractal design may be an excellent alternative the modeling, simulation, and fabrication is believed to be more complicated than the MSAA. Hence, this work investigates design of the MSA and MSAA.

## 1.3 Hypothesis

This thesis investigates the design of an inset-fed MSAA. The design uses a quasi log-periodic microstrip antenna method (LPMSAA). The LPMSAA will be for wide-band operation in continuous-wave applications. The underlying hypothesis is that the LPMSAA can be designed to operate from X through Ka bands while still meeting low SWaP requirements. The approach is to analyze recently reported designs using $\lambda/2$, square patch elements, co-linearly arranged with a linear inset feed. The transmission line model is used to determine coarse design dimensions and antenna simulation is performed to refine the design. Following the simulation and analysis, a LPMSAA will be constructed on a

suitable substrate and tested.

Thus, the motivation for our antenna is to provide the necessary, fractional bandwidth to cover 80% of X, Ku, K and Ka bands, that is 8-40 GHz with one multiple element, inset feed, LPMSAA. The desired $BW$ will be approximately 80% to 133%. The above $BW$ is based on a center frequency of 24 GHz. The said antenna will also have a 3-dB beamwidth $<$20 degrees, gain $>$ 3-dB, VSWR $<$1.8, over the entire $BW$.

## 1.4 Outline of Thesis

This paper is organized into 5 chapters. Chapter 1 consists of the introduction to the antenna problem, motivation, challenges, and hypothesis. Chapter 2 provides a survey of the literature on the LPMSAA. Chapter 3 consists of the methods used to simulate, fabricate, and design the antenna. Chapter 4 presents the results of research. An finally, the conclusions, summary, and recommendations for future work are presented in Chapter 5.

# 2 Background

## 2.1 Log Periodic Antenna Design

The Log Periodic Antenna (LPA) was first introduced by DuHamel and Isbell in 1957. The most important principle consists of designing the antenna structure so that its parameters are scaled periodically with the logarithm of the frequency [10]. However, this principle is somewhat misleading. The antenna parameters are typically scaled by a factor called $\tau$. The main idea behind a log periodic antenna is that its dimensions will scale by this constant factor and the antenna becomes increasingly wide-band, and almost limitless in bandwidth, as long as elements are continually added. The authors discuss three basic design principals, of which scaling the antenna structure is the most interesting and widely used concept. The other two concepts are not relevant to this paper and can be found at [10].

Since only one of these design principles is employed in this paper, the LPMSAA is called "quasi-log periodic".

The Log Periodic Method has been presented in many papers, as noted below. Log periodic arrays are also very popular in dipoles and many other types of antennas. This research focuses on wide $BW$, but many novel antenna designs exist for other purposes: dual band, directive, pattern and polarization specific, efficiency, and so on. The design method used by authors cited here is the transmission line method. The transmission line method is a simplified approach to design the patch length, width, inset depth, frequency and feed line as in (2). Basically, the transmission line method is used to design the first element ($m$ element). Each subsequent element is called the $m+1$, $m+2$,.. element. Each element is a square patch with length ($L$) and width ($W$) equal, that is $L = W$. The subsequent elements are scaled by a scaling factor $\tau$, or sometimes called $k$. Some designers have been known to use a scaling factor of $\tau = 1.05$ or even greater. It is up to the individual and the required frequency spacing requirements. Since individual patches are so narrow in bandwidth, $\tau = 1.05$ is reasonable.

$$\tau = \frac{f_{m+1}}{f_m} = \frac{L_{m+1}}{L_m} = \frac{W_{m+1}}{W_m} = \frac{I_{m+1}}{I_m} \tag{1}$$

$$\log(\tau) = \log\left[\frac{f_{m+1}}{f_m}\right]. \tag{2}$$

The Log Periodic Method has been used to achieve very wide $BW$s in patch antenna arrays but for lower frequency ranges. In [11] the author described the design and simulation results for five, seven and nine element quasi-log periodically scaled MSAs. These designs are within the frequency range of 2.03-3.01 GHz. The five, seven, and nine-element antenna $BW's$ are 22%, 33%, and 44%, respectively. As the number of elements increase, so does the opportunity to increase $BW$. In the same band, a $BW$ of 51% was achieved with nine-elements [12]. The antenna design was simulated and fabricated. The simulation results are compared to the measured results. Finally, in [6] a $BW$ of 98% was attained for

the UWB short-range wireless communication band of 3.1-10.6 GHz.

Log periodic antenna arrays are very popular and sometimes necessary due to the wide $BW$ and frequency independence requirement. Other popular designs are in conjunction with Koch Fractals, which can potentially decrease the array size [13]. The author here used a proximity feed where square patches were laid out over a substrate with a feed line beneath. In regards to continuing work on the subject, the log periodic method is still popular. Log periodic dipoles are very popular today and are used in the industry in many ways. The MSAA with square patches is not a new concept as the design principle has been around for over 60 years. The most recent research found has been related to the more popular rectangular patch antenna and various array structures. A simple internet search results with many novel and interesting designs related to this subject. Conformable designs, triangular patches, and various other feed styles are also very popular for patch antennas. IEEE literature includes much more information. Perhaps the log periodic method with square patches is not pursued exactly as presented here, but in different forms, triangular patches, con-formal designs, etc. One of the latest papers is from 2011 [14]. Miniaturization is very popular, therefore fractals may be of more interest. Patch antenna arrays are not going away, however they lack efficiency and may not have the high directivity of the ubiqutous dipole element style array.

## 2.2 Patch Antenna Design

### 2.2.1 Design

There are many variations to the geometry of a MSA, of which the design and desired radiation pattern, $BW$, gain, directivity, input impedance, etc, all play a role in it's structure. A popular starting choice for a single patch antenna is the $\lambda/2$ rectangular microstrip antenna (RMSA). A RMSA can be modeled as a rectangular copper patch on top of a substrate of thickness $t << \lambda$ with permittitvity $\epsilon_r$, and backed by a large ground plane, as shown in Figure 1. The feed is a microstrip transmission line. The patch has a length $L$ and width

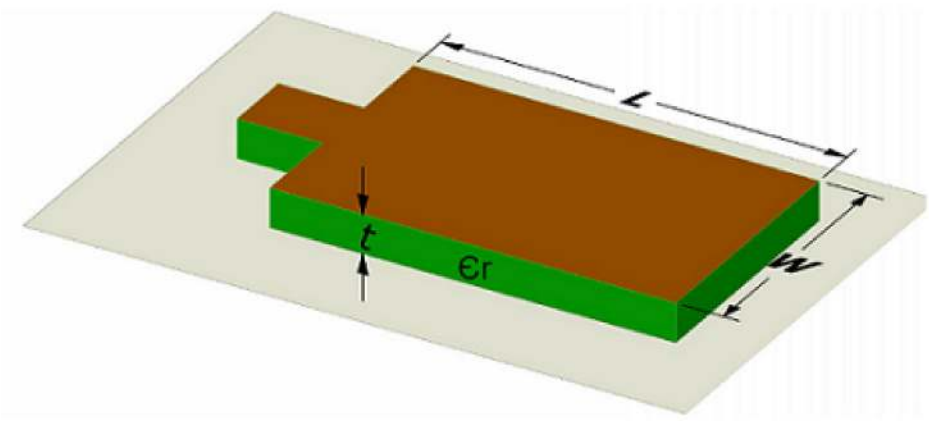


Figure 1: Sketch of RMSA on large ground plane.

$W$. When the patch length is approximately $\lambda_d/2$ with respect to the wavelength in the dielectric, the patch becomes resonant with an input reactance $X \approx 0$. A RMSA is generally accepted to have a maximum $8\% - 12\%$ $\%BW$ [5, p. 466] where fractional bandwidth or $\%BW$ is defined as

$$\%BW = \frac{100BW}{f_c}\,, \tag{3}$$

and raw $BW$ is

$$BW = f_u - f_l\,,\ \text{(Hz)} \tag{4}$$

$$f_c = \frac{(f_u + f_l)}{2}\,,\ \text{(Hz)} \tag{5}$$

where $f_c$ is the center frequency, $f_u$ and $f_l$ are the upper and lower frequency limits respectively, of the antenna $BW$ requirements [5, p. 218]. RMSAs or square MSAs can be connected to the feed network in many different ways. Some of the more popular approaches are "coaxial, stripline, aperture-coupling, or proximity coupling-methods" [15]. The selected method depends upon the application and desired design parameters.

The $BW$ of an antenna is the inverse of it's quality factor $Q$ [2, p. 11]

$$BW = \frac{VSWR - 1}{Q\sqrt{VSWR}}. \tag{6}$$

Voltage standing wave ratio, $VSWR$, is a measure of the amount of wave reflection caused by impedance mismatches. A $VSWR$ of 1 is ideal, that is, the antenna would have no mismatches or reflections. $VSWR$ is defined as [2, p. 11]

$$VSWR = \frac{1 + |\Gamma|}{1 - |\Gamma|}, \tag{7}$$

where $\Gamma$, the reflection coefficient can be defined as [16, p. 57]

$$\Gamma = \frac{V^-}{V^+} = \frac{(Z_L - Z_0)}{(Z_L + Z_0)}. \tag{8}$$

The reflection coefficient $\Gamma$, is also used to determine the return loss of impedance mismatches. When the load impedance does not match the input impedance and/or characteristic impedance of the transmission line, the circuit will have a reflected voltage wave $V^-$. The magnitude of this loss is called return loss $R_L$ and is defined by [16, p. 58]

$$R_L = -20 \log_{10} |\Gamma|. \quad dB \tag{9}$$

The reflection coefficient can be determined using a vector network analyzer. Network analyzers can be used to measure scattering parameters or commonly called s-parameters making the return loss measurement simple to estimate the antenna's return loss as in (10) [16, p. 179]

$$R_L = -20 \log_{10} |S_{11}|. \quad dB \tag{10}$$

"The $BW$ is usually specified as frequency range over which $VSWR < 2$ (which corresponds to a return loss of 9.5 $dB$ or $11\%$ reflected power)" [2, p12,37].

### 2.2.2 BW Enhancement Techniques

There are many techniques that can be employed to increase the $BW$ of the patch antenna. The most obvious one would be to increase the width and length of the patch for the phys-

ical size is directly proportional to $BW$, but that would defeat the purpose of a low size and weight antenna. A single patch MSA can have an extended $BW$ of up to $20\%$ by simply increasing the height of the substrate to $0.15\lambda$. An experimental equation for $BW$ at resonant frequencies, and $t \leq 0.15\lambda$ can be found in (11) [5, p. 471]

$$BW = 3.77 \frac{\epsilon_r - 1}{\epsilon_r^2} \frac{W}{L} \frac{h}{\lambda}. \quad t \ll \lambda \tag{11}$$

An increase in substrate height, $h$ or the patch width, $W$ would increase the overall $BW$ with the provided constraints. Essentially, an increase in the height leads to broader fringing fields along the width edge of the patch (fringing fields will be discussed in more detail in chapter 2.2.9). However, one could increase the height, but this can lead to an increase in the power of surface waves and decrease in the power of radiation. Also, this can lead to sub-par radiation efficiency [17]. The $BW$ could also be manipulated by altering the patch geometry (see Figure 2) such as introducing one or more slots inside the patch at appropriate locations. The author here was able to increase the $BW$ of a rectangular patch by increasing the substrate height and truncate the corner. The $BW$ was further increased by $21.2\%$ by adding a routed H slot. The third iteration was to add a U slot which further increased the $BW$ up to $50.7\%$. The slots inside the patch increase the $BW$ by adding modes near the fundamental mode [18].

Consideration should be given to the use of the substrate dielectric constant. The dielectric constant, also known as the relative permittivity, $\epsilon_r$ plays a significant role in the patch antenna's $BW$. There are numerous substrates that can be used for the design of microstrip antennas. The range of dielectric constants are typically from $2.2 \leq \epsilon_r \leq 12$. The substrates with good antenna performance are thick and whose dielectric constant's are on the lower end of the above range. Substrates with this design provide better efficiency, wider bandwidth, and loosely bound fields for radiation into space, but at the expense of a larger element [17]. Alternatively, in ideal circumstances, it would be best to use a high

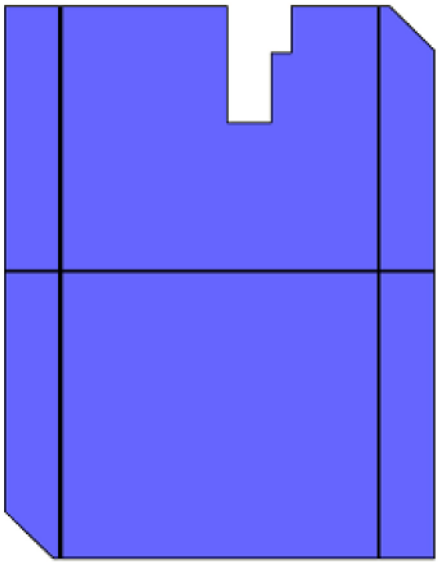

Figure 2: Tuncated patch antenna with H and U slots.

dielectric constant substrate for the feed lines. However, if one is to use microstrip lines to feed the patch, it makes sense to use the same substrate for the feed as well as the patch antenna.

The dielectric constant can be thought of from a conceptional point of view as being directly proportional to the "tendency to retain electric fields". Low dielectric constant leads to wider $BW$ and less retention of fields whereas high dielectric constant leads to stronger retention of fields [17].

### 2.2.3 Feeding Methods

There are numerous ways to feed a MSA [4, p. 813]. The inset microstrip feed method is used here because it is economical to fabricate and simple to design and simulate. Many of the papers researched here use this same feed method. For optimal $R_L$, the microstrip feed line characteristic impedance ($Z_0$) must match, as close as possible, the input impedance of the patch. The microstrip feed line should not produce a field pattern because it is small compared to the wavelength of the patch center frequency ($f_0$) [5, p. 469].

The estimated characteristic impedance of the feed microstrip can be calculated as fol-

lows in (12) and (13) [4, p. 825]

$$Z_0 = \frac{60}{\sqrt{\epsilon_{eff}}} \ln\left[\frac{8h}{W_0} + \frac{W_0}{4h}\right], \quad \frac{W_0}{h} \leq 1 \tag{12}$$

or

$$Z_0 = \frac{120\pi}{\sqrt{\epsilon_{eff}}\left[\frac{W_0}{h} + 1.393 + 0.667\ln\left(\frac{W_0}{h} + 1.444\right)\right]}. \quad \frac{W_0}{h} \geq 1 \tag{13}$$

The height of the substrate ($h$) is typically already known due to the selection of substrate materials available for fabrication. The ratio $W_0/h$ can be determined by using (14), (15), (16), and (17) [19] [16, p. 148-149]

$$\frac{W_0}{h} = \frac{8e^A}{e^{2A} - 2}, \quad \frac{W_0}{h} \leq 2 \tag{14}$$

or

$$\frac{W_0}{h} = \frac{2}{\pi}\left[B - 1 - \ln(2B-1) + \frac{\epsilon_r - 1}{2\epsilon_r}\Big(\ln(B-1) + 0.39 - \frac{0.61}{\epsilon_r}\Big)\right], \quad \frac{W_0}{h} \geq 2 \tag{15}$$

$$A = \frac{Z_0}{6}\sqrt{\frac{\epsilon_r + 1}{2}} + \frac{\epsilon_r - 1}{\epsilon_r + 1}\left(0.23 + \frac{0.11}{\epsilon_r}\right), \tag{16}$$

$$B = \frac{377\pi}{2Z_0\sqrt{\epsilon_r}}. \tag{17}$$

### 2.2.4 Voltage and Current Distribution

An antenna radiates electromagnetic fields into space via accelerated charges. Accelerated charges radiate when there is a change in direction or speed. As charges move back and forth along the copper trace of the patch acceleration occurs and an electromagnetic field is generated normal to the charge direction. Since antennas are typically open circuits, charges can accelerate when they reach the end of the antenna trace or wire. Antennas are typically fed with a sinusoidal signal which creates time varying charges in the patch. The

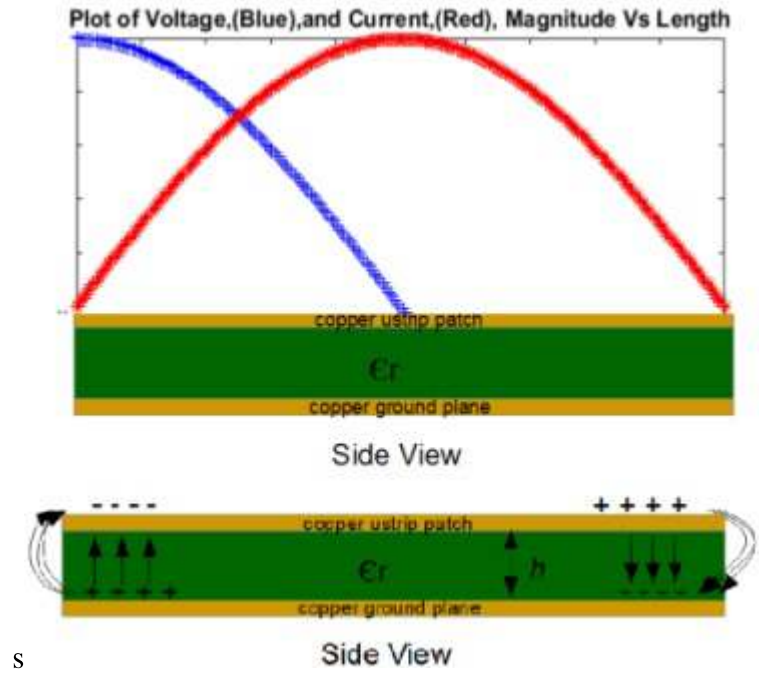


s

Figure 3: Simulated voltage and current distribution on patch antenna.

electromagnetic waves continue to travel into space, at the speed of light, away from the accelerated source [5, p. 14].

An intuitive explanation to the patch antenna radiation can be explained as below. The fringing fields are a result of the uneven, sinusoidal voltage distribution throughout the patch antenna, see Figure 3 and equations (18), (19), and (20). Clearly, the voltage and current are out of phase [17]

$$V(x) = V_0 \cos \frac{x\pi}{L}, \tag{18}$$

$$I(x) = \frac{V_0}{Z_0} \sin \frac{x\pi}{L}, \tag{19}$$

$$Z_{in} = \frac{V(x)}{I(x)}. \tag{20}$$

Since the patch is an open circuit, all the incident voltage, $V^+$ is reflected back as $V^-$, therefore $|V^-| = V^+$ thus the reflection coefficient, looking into the antenna, $\Gamma = 1$ as per (8). Theoretically, the current at the feeding and opposite edge will be a minimum whereas the current at the middle of the patch will be at a maximum. The current on the top con-

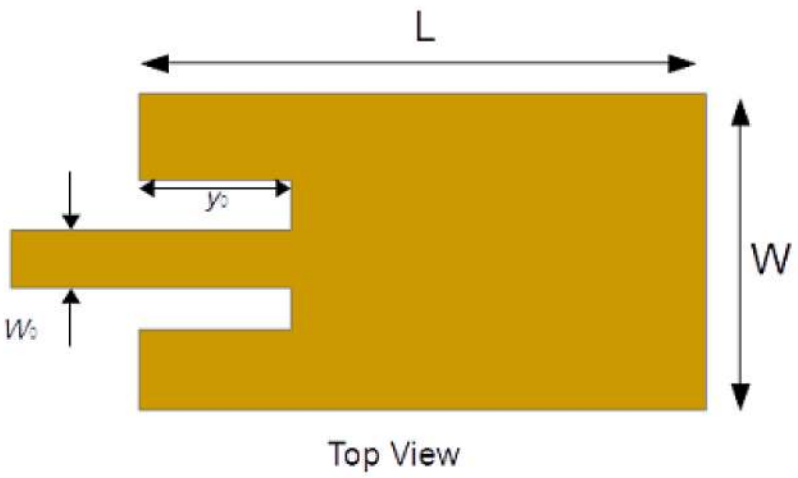


Figure 4: Microstrip patch antenna with inset depth, $y_0$.

ductor of the patch cancels with an equal magnitude and opposite phase current in the ground plane conductor. Therefore, the fields directly below the patch that are a result of the equal but opposite current distribution cancel out, similar to an ideal transmission line. Conversely, the voltage is a maximum $V+$ at the feeding edge and minimum $V-$ at the opposite edge. The patch is essentially an open circuit and the negative lower voltage $V^-$ at the end of the patch produces an attractive negative charge. Whereas the $V^+$ voltage at the feed end of the patch produces a repelling, positive, charge. The charges directly beneath the patch, are equal and opposite, and cancel out. Any residual fields between the patch top conductor and the ground plane cancel as they travel in the opposite direction. Therefore, no electromagnetic fields will be produced directly below the patch and consequently the fringing fields at the ends of the patch envelope on top of the patch and create a broadside radiation pattern. In summary, the voltage distribution leads to a distinctive charge distribution which leads to fringing fields and thus causes the radiation pattern as described above [20].

### 2.2.5 Input Impedance

The input impedance of the patch antenna has two parts, $R$ is the real resistance part and $X$ is the reactance [4, p. 80]

$$Z_{in} = R + jX. \tag{21}$$

At resonance, the frequency=$f_0$, antennas have a unique property where the reactance $X$ will be very close to zero and is considered negligible [5, 468]. Therefore, we can calculate the resonant input resistance as $R_{in}$, the real part, at the point $y = 0$ from the feeding edge of the patch. Normally, the input resistance at the edge of the patch will be very high. The high input resistance is due to voltage, current distribution according to Ohms Law. The expected $R_{in}$ at $y = 0$, should be approximately 200-400 Ohms. As per (22), one can reduce the antenna input impedance by moving the feed line slightly toward the center of the patch. Each element will be fed with a 100 Ohm transmission line. Transmission lines have maximum power transfer with a matching load, that is, with the load impedance ($Z_L$) equal to the characteristic impedance $Z_0$. Of course, it is preferred that no reflections are generated on a transmission line. Therefore, in the ideal case, the reflection coefficient $\Gamma = 0$, but in the real world, it is impossible since transmission lines are typically reactive and lossy.

It is necessary to calculate the required patch inset depth to attain a 100-Ohm input resistance at $y = y_0$, see Figure 4. $R_{in}$ is based on the conductance of the microstrip radiator, $G_1$, the mutual conductance between the two radiating slots, $G_{12}$, and the distance between the radiators, $L$, as shown in Figure 5, and calculated using (22-26)

$$R_{in} = \frac{1}{2(G_1 \pm G_{12})} \cos^2(\frac{\pi y_0}{L}). \tag{22}$$

One can set $y_o = 0$ to find $R_{in}$ at the edge, or more directly set $R_{in} = 100$ and solve for $y_o$. If the patch length is chosen to be $\lambda/2$, that is, with the fringing length added, then the

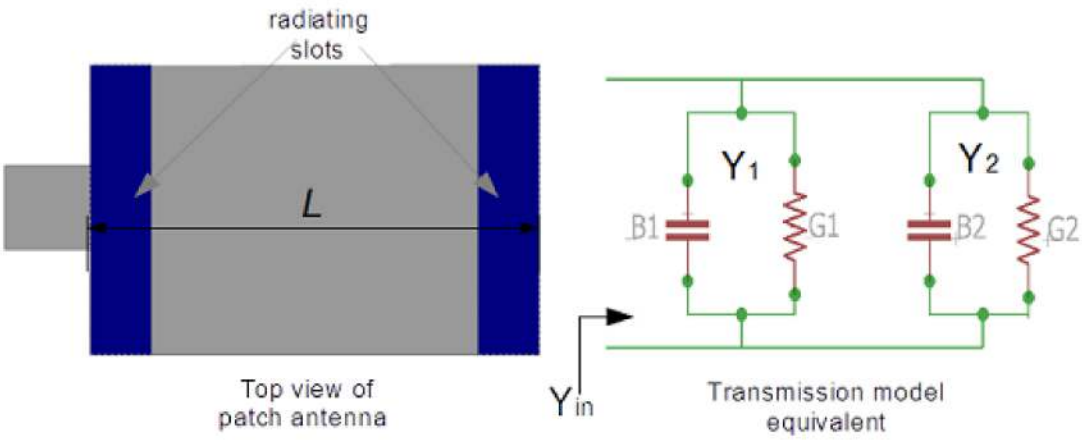


Figure 5: Radiating slot apertures and equivalent circuit of slot conductance.

input admittance will be real

$$G_1 = G_2, \quad B_1 = B_2 = 0, \tag{23}$$

$$Y_{in} = Y_1 + Y_2 = 2G_1. \tag{24}$$

$G_1$ is the microstrip conductance and can be found from

$$G_1 = \frac{1}{120\pi^2} \int_0^{\pi} \left[ \frac{\sin\left(\frac{k_0 W}{2}\cos\theta\right)}{\cos\theta} \right]^2 \sin^3\theta d\theta, \tag{25}$$

$G_{12}$ is the mutual conductance between the two outer slots [4, p. 820-825] [11],

$$G_{12} = \frac{1}{120\pi^2} \int_0^{\pi} \left[ \frac{\sin\left(\frac{k_0 W}{2}\cos\theta\right)}{\cos\theta} \right]^2 J_0\left(k_0 L \sin\theta\right) \sin^3\theta d\theta, \tag{26}$$

where "$J_0$ is the Bessell function of the first kind order zero" [12].

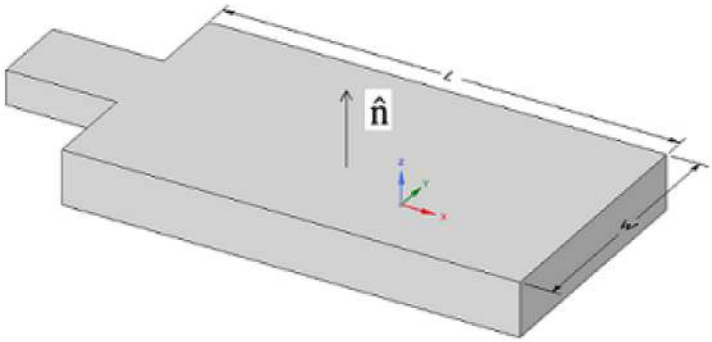


Figure 6: Direction of wave propagation, normal to patch.

### 2.2.6 Radiation Pattern

Patch antennas generate a radiation pattern that is broadside, normal to the patch, in the n̂ direction. Figure 6 shows the direction and Figure 7 shows an example pattern. This unique property is the result of the fringing fields, the ground plane below, and half wavelength separation of primary radiating slot apertures. Patch antennas are inefficient radiators because only the two slot apertures form the primary radiating structure. The radiation pattern can be best described through simulation. However, a general theory of the formation of patterns can be formulated through the use of equivalence principles and treating the two radiating edges, along the width, as slot apertures. There are four sides that can radiate the pattern, two along the length and two along the width. The two sides on the length of the patch may radiate as well, but the radiated fields are normally considered negligible. Image theory can be used to explain the radiated fields (27)

$$\vec{M}_s = -2\hat{n} \times \vec{E_A}. \tag{27}$$

$\vec{M}_s$ and $\vec{E_A}$ are the equivalent magnetic current density and electric field, respectively. The factor of $2$ is from the image of the magnetic current in the ground plane and $\hat{n}$ is the unit normal vector (Z-axis). Assume that with equivalence principles, [4, ch. 12.2], the two slot apertures are to produce equal magnitude and in phase radiation and radiate as magnetic

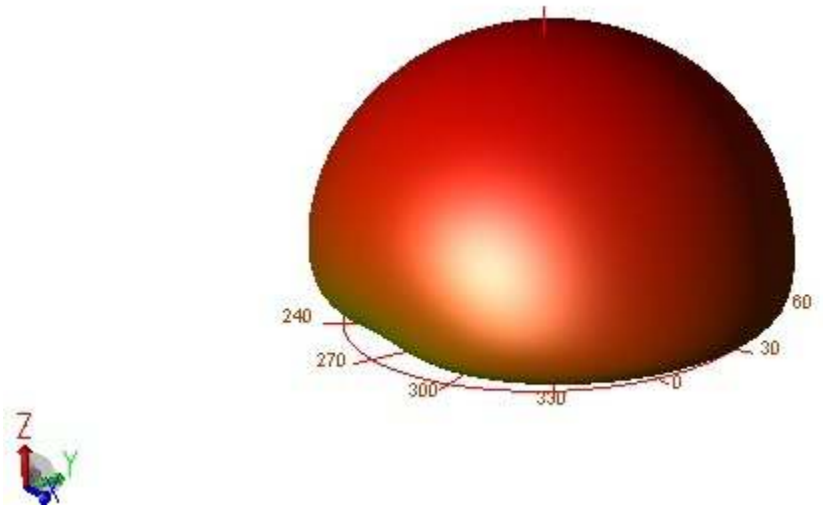


Figure 7: 3D, Square patch antenna simulation pattern from ADS MoM.

antennas with each having one unit of $\vec{M}_s$. The radiating slots become a two-element array, separated by a transmission line of approximately 1/2 $\lambda$, which causes a phase reversal, which leads to radiation in the $\hat{n}$ direction [4, pp. 832-834].

The spherical coordinate system is specified in terms of $\theta$ and $\phi$ for a point in space that is distance, $r$, from the center of the antenna. Essentially, the far-field approximation in spherical coordinates is the expected end result because the fields radiated by antennas are typically radiating away spherically, Figure 8. The patch antenna ground plane acts like a mirror to reflect any radiated image therefore, very little radiation comes from below the ground plane, thus radiation is limited from $90 \leq \theta \leq -90$ and $0 \leq \phi \leq 360$ degrees. The patch antenna is said to have a theoretical front-to-back ratio of $100\%$. The general far-field approximation for a rectangular patch can be found at [5, p. 470]. An alternative detailed description for a cavity model with TM modes for rectangular patches can be found at [4, ch. 14.2.2 ]. Unfortunately, the far-field approximation equations for square patches was not found. In addition, the simulation of an RMSA pattern for a single square patch at 8.1 GHz can be seen in Figure 7.

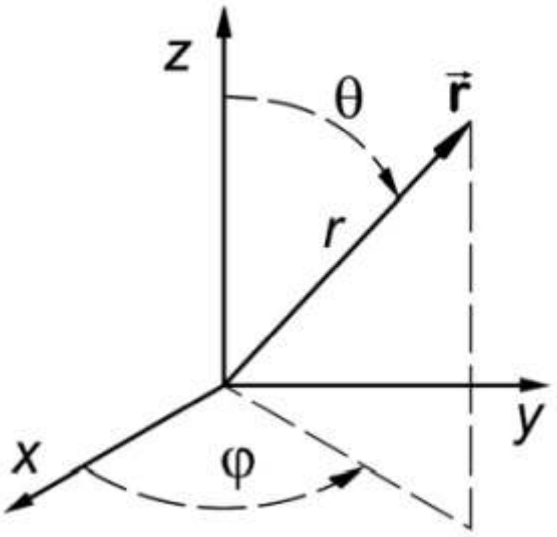


Figure 8: Spherical coordinate system, (source: Datei:Spherical polar coordinates.png, de.m wikipedia.org).

### 2.2.7 Transmission Line Design Method

The transmission line method is used in many papers and texts to design patch antennas. The process is explained and used in [4, 6, 9, 11, 12]. First, the authors estimated the width, $W$ of the patch. This is a relatively accurate method to begin the design process

$$W = \frac{\lambda_o}{2}\sqrt{\frac{2}{\epsilon_r + 1}}, \tag{28}$$

where $c$ is the speed of light in free space, $f_0$ is the frequency of operation and $\lambda_0$ is the free space wavelength

$$c = 3 \times 10^8, \text{ m/s} \tag{29}$$

$$\lambda_0 = c/f_0. \tag{30}$$

### 2.2.8 Effective Permittivity

For patch antennas, the electromagnetic field lines on the fringe of the width, are not in a completely homogeneous environment. The field lines are above the patch at first, in the air, then bend downward towards the ground plane and into the substrate. The substrate will

ultimately refract the field lines. Consider that the substrate will have a relative permittivity, ($\epsilon_r$) as defined by the supplier, ie Rogers. However, for simulation purposes, we can assume the permittivity will vary, due to the inhomogeneous environment and the height, $h$, and width, $W$, of the patch substrate material. The thickness of the microstrip line is considered miniscule and not normally factored into this equation. One must calculate the effective permittivity, $\epsilon_{eff}$, as a function of these factors [4, p. 816-817], [16, p. 148], [11, 21]

$$\epsilon_{eff} = \frac{\epsilon_r + 1}{2} + \frac{\epsilon_r - 1}{2} \frac{1}{\sqrt{1 + 12\frac{h}{W}}}. \tag{31}$$

### 2.2.9 Fringing Effect

The fringing fields along the width of the patch make the patch electrically longer. This is called the "Fringing Effect" (see Figure 9). The patch will radiate at a lower frequency unless compensation to the patch length $L$ is accounted for. The fringing effect will vary the electrical length of the patch and is called the effective length, $L_{eff}$. The antenna will appear to be longer than the physical length $L$. The additional fringing length can be estimated as $\Delta L$ [4, p. 818-819] [11, 21]

$$\Delta L \approx 0.412h \frac{\epsilon_{eff} + 3}{\epsilon_{eff} - 0.258} \frac{\frac{W}{h} + 0.264}{\frac{W}{h} + 0.8}, \tag{32}$$

The overall electrical length of the patch antenna can be estimated as $2\Delta L + L$.

### 2.2.10 Resonant Frequency

The approximate resonant frequency for a rectangular or square patch antenna can be re-calculated as $f_0$, as in (33). For the research here, a square patch with $L = W$ will be created [11, 21], [4, p. 819]

$$f_0 = \frac{c}{2(L + 2\Delta L)\sqrt{\epsilon_{eff}}}. \tag{33}$$

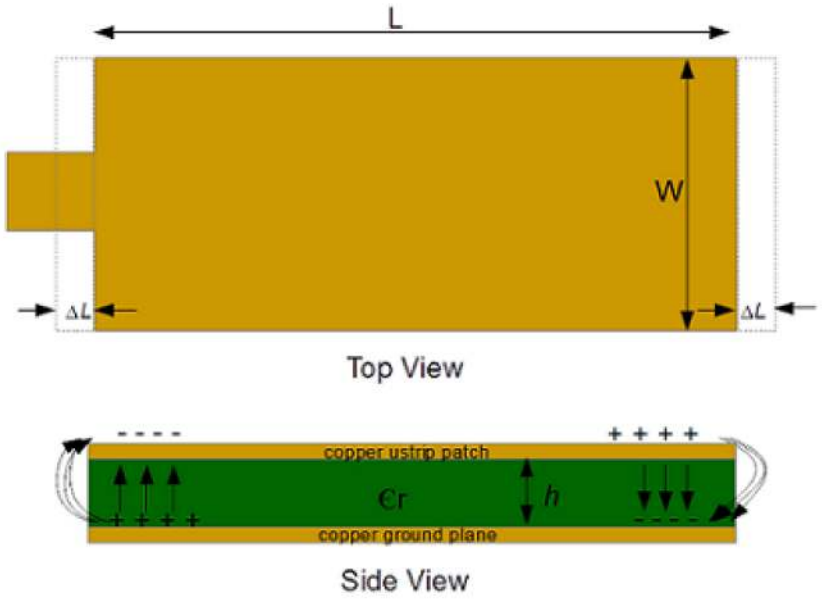


Figure 9: Microstrip patch antenna showing fringing effect and charge build up.

### 2.2.11 Feed Line Length

Since the electromagnetic field flux lines are partially in air and the majority are in the substrate, the propagation velocity and wavelength of a plane wave will be less than as if it were in free space. One must estimate the variation of the wavelength, $\lambda_g$, in this case of in-homogeneous environment

$$\lambda_g = \frac{\lambda_0}{\sqrt{\epsilon_{eff}}}. \tag{34}$$

$\lambda_g$ is to be estimated for each patch, based on the value of $\lambda_0$ as in (30) [19]. Following the calculation of $\lambda_g$, one must calculate the feed transmission line length for each patch. The length of the branch transmission line feeding the patch array is a critical length called, $d_m$. The aggregate sum of $d_m$, $I_m$ and the main transmission line, is to be a multiple of $\lambda_g/2$ for the patch in question [22]. The motivation for this requirement is that for $\lambda_g/2$ or any multiple thereof, the input and output impedance will be equal. This will create the opportunity for maximum power transfer [16, p. 58]. In most literature $d_m$ is shown as the offset distance from the $I_m$ branch line between the $m$ and $m+1$ elements. The overall

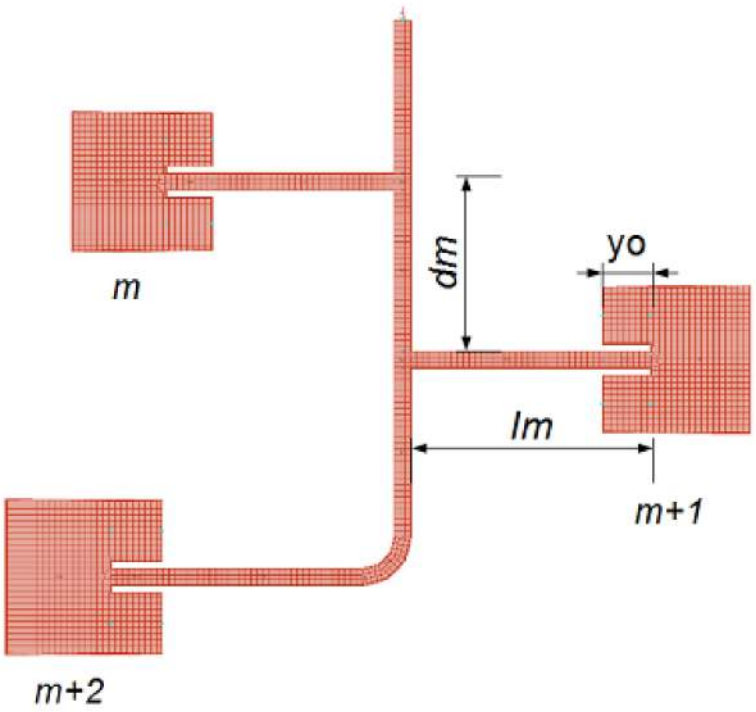


Figure 10: Partial drawing of collinear array.

transmission line length can be calculated from

$$\frac{n\lambda_g}{2} = d_m + I_m + \text{main trunk line length.} \quad n = 2, 4, 6, 8... \tag{35}$$

$I_m$ is the offset distance from the main trunk transmission line. $I_m$ is not a critical length, but the patch needs to be offset from the main transmission line such to reduce coupling, see Figure 10. In order to limit or filter resonant waves to each patch, the transmission line plays a role in limiting pass band signals. The length of the $m + 1$ element $d_m$ section, must be such that higher frequency waves that are meant for the $m$ element are impeded by an open or high impedance circuit to the $m + 1$ patch [11]. The adjustment to the transmission line length is primarily a function of $d_m$. The logical choice for $d_m$ is the shortest length possible, such to reduce insertion loss of the feed transmission line and to achieve the smallest footprint possible [22].

### 2.2.12 Modes, Polarization, Efficiency, Gain, Pattern, Directivity

Square patches are used to limit the higher order modes that can be detrimental to our ideal radiation pattern. In addition, polarization and efficiency will be further affected by higher order modes [11, 21]. The ever-popular rectangular patch antenna element is believed to be emit TM (transverse magnetic) fields, thus TM fields are often called electric waves because the electric field is in the direction of the wave propagation. With TM fields, the magnetic component is tangential to the direction of the radiated wave [4, pp. 828-831].

Since antennas are used for communication over long distances, typical parameters such as gain, directivity, efficiency, radiation pattern, beamwidth, polarization, etc, should also be determined and reported in the far-field. The far-field line of sight distance, for most applications can be estimated as [4, p. 35], [5, p. 43]

$$R \geq \frac{2D^2}{\lambda}. \tag{36}$$

A simple rule of thumb for the far-field distance has also been known as $R \gg \lambda$ or approximately $10\lambda$ [23]. In the far-field, electric and magnetic field vectors will be orthogonal to each other. As the radiated wave approaches infinity, the wave front will theoretically be plane-like and have a more consistent even front, thus, traveling away from the antenna in the radial direction. The magnitude of the wave front, normally expressed in dB, will be equal over the lobes of the pattern [4, p. 72]. Conversely, waves in the near field will not be plane, and furthermore, the electric and magnetic field vectors are not expected to be orthogonal to each other. For the discussion here, all parameters are observed in the far-field.

The gain of an antenna is typically specified in reference to an ideal antenna source such as an isotropic, or spherical equally-radiated antenna (see Figure 11). The isotropic antenna does not exist in nature, but it provides a reference gain that is used by nearly all antenna manufacturers. Therefore, gain can be specified in dBi (dB over isotropic). One can also

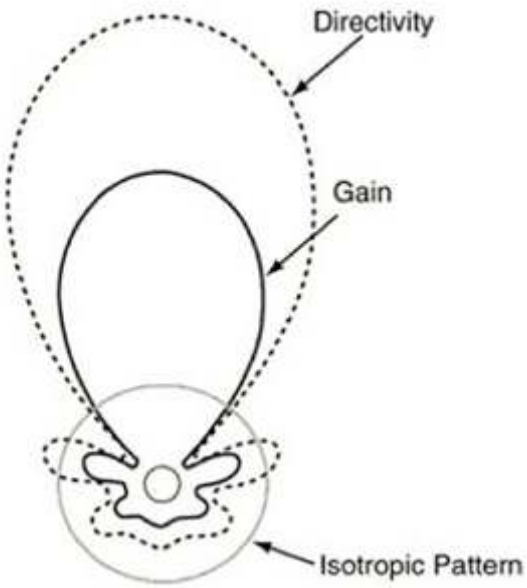


Figure 11: Drawing depicting gain and directivity, (source: Digikey, https://www.digikey.com/en/articles/techzone/2017/apr/understanding-antenna-specifications-and-operation).

use the ubiqutous dipole antenna gain as a reference, this could be especially helpful for dipole designs. Nonetheless, it is up the individual's preference. Gain is specified to have a magnitude and direction (angle). The absolute gain of an antenna, $G$ is the product of the efficiency and directivity, and calculated as [24], [4, p. 67]

$$G = e_0 D. \tag{37}$$

Should the antenna be 100% efficient then the gain would be equal to the directivity [25, p. 17]. For spherical coordinates the gain and directivity vectors can be specified in terms of $\theta$ and $\phi$. The efficiency is an expression usually given as a ratio of the amount of power delivered through the antenna. Efficiency can also be expressed in percentage of power delivered. Typically, efficiency takes into account the losses associated with mismatches at the connector and power losses in the antenna itself. The total efficiency, $e_0$ is defined by

$$e_0 = e_r e_c e_d \,, \tag{38}$$

and

$$e_r = 1 - |\Gamma|^2 , \tag{39}$$

where $e_r$ is the reflection mismatch loss, $e_c$, and $e_d$ are the conduction and dielectric power losses respectively [4, p. 65]. Albeit, the individual efficiency terms above would be difficult to determine however, $e_0$ is more likely to be obtained analytically.

The directivity is simply the maximum radiation intensity, $U_{max}$, in a specified direction, divided by the average radiation intensity, $U_{avg}$, of the entire radiation pattern. Directivity is unitless, usually noted on a polar plot, or can also be specified in terms of $\theta$ and $\phi$ [5, p 52]

$$D = \frac{U_{max}}{U_{avg}}. \tag{40}$$

It is also intuitive to think of a highly directive, or high gain antenna as most of the power is radiated or received from one direction. The antenna is a very directed source or receiver that is, most of the radiation is concentrated into a single direction or beam. A log periodic, horn, or parabolic antenna are examples of highly directive antennas. Conversely, an antenna that is not highly directive typically has it's radiation more evenly distributed spherically. Such an antenna would be better suited for cell phone communication. Examples of such would be dipole, monopole, or meander pcb trace antennas. The polarization of the antenna is simply the polarization of the radiated wave emitted by the antenna in a given direction. Alignment of antennas is very important; this is called polarization match. Polarization match is when the transmit and receive antennas are oriented such that the polarization of the plane wave emitted from the transmitter matches the polarization of the receiving antenna [25]. RF sources such as TV and radio stations, have output power up to 50,000 Watts, for long distance transmission. For best reception, it makes sense to align the receiving antenna in the same polarization, to have the most power transfer possible. RF devices may still work, if the antenna polarities are not matched or aligned, however, there will be a lower field strength and therefore the distance between devices might have

to be reduced in order to communicate properly. In the above case, one could be near the maximum of the link budget of the entire RF path. The polarization of the antenna is defined by how the radiated electromagnetic wave will travel in space and time. The wave will have a electric and magnetic field components, but for discussion here, consider only the electric field component. The electric field can be described as a vector with magnitude and direction. How the electric field travels is denoted also as the polarization of the wave front (plane waves). Essentially, there are three types of wave polarization's: linear, circular and elliptical. If the electric field vector is directed in a straight line as it travels through space, throughout the propagation of the wave front, the field is described as being linearly polarized. Similarly, if the electric field vector creates a circular or elliptical path, then the field is described as being circular or elliptically polarized respectively [4, p. 72].

### 2.2.13 Test and Analysis of Results

The conventional method of creating the initial design is to use the above equations to design the antenna. The equations will provide an initial idea of what the antenna will look like. The next step would be to lay the design out in a schematic capture program, in this case ADS, and then to simulate using ADS Momentum MoM with a low mesh of 10 cells per wavelength. For the simulation to be as accurate as possible one should create a stack-up for the pcb (Figure 12). The stack-up would specify the laminate material, loss tangent, dielectric constant, copper thickness, and more. When the simulation is complete, the parametric sweep is normally displayed with $S11$ in log magnitude and phase format. The data showss the $R_L$ and phase shifts verse frequency, for the pass band of the antenna. Phase shifts occur at resonance points. The simulation data is helpful to make decisions regarding moving forward with fabrication, or redesigning. To determine impedance mismatches, the input impedance versus frequency can be plotted and analyzed as needed. The far-field analysis should be completed to verify the radiation pattern for co and cross polarization characteristics. One can also collect 2-dimensional slices for the three planes,


Figure 12: ADS stack-up of FR-4 for patch antenna array.

XY, XZ, and YZ. With the 2-dimensional slices, the gain, efficiency, directivity, and half power beamwidth can be determined. A 3-dimensional plot is also helpful to determine what the overall radiation pattern looks like. The above is only a short description of what can be simulated. Finally, fabrication of the antenna and a side-by-side comparison of the simulated versus empirical results would suggest the accuracy of the simulation.

## 2.3 Technical Challenges

### 2.3.1 Antenna Design Challenges

The greatest challenge is the large bandwidth requirement of 133%. The designs presented in Chapter 2.1 utilize FR-4, which is a low cost medium grade, fiberglass substrate with an approximate relative permittivity, $\epsilon_r = 4.7$. FR-4 is an economical, general-purpose substrate that is ubiquitous in the pcb fabrication industry. It is typically used for patch antenna designs in the sub 10 GHz band.

A more aggressive approach to the antenna design is necessary to achieve the goals required. For a wide as possible bandwidth a much lower dielectric constant is preferred. Rogers Duroid 5880 substrate material has a dielectric constant of approximately 2.2 and 1.57 mm substrate height. Duroid also has 35 micron top cladding (1 oz/sq ft) and loss tangent of 0.0009. Rogers 5880 will allow a wider bandwidth to be attained.

The author in [4, pp. 820-825] explains the conductance and input impedance equations in detail, (21) through (26) above. However, the equations are for rectangular patches. The papers, [6, 11, 21] use similar equations to design a square patch array to match the 50-

Ohm transmission line, so some interpolation was required. Another issue discovered is that with low relative permittivity substrates like Rogers Duroid 5880, the characteristic impedance of the feed microstrip lines will be a bit higher at approximately 70 Ohms for 3 mm width, as per (12) and (13). This will be a problem for a few reasons. First, the patch input impedance is normally inset for $Z_{in} = 50$ Ohms. Second, as the resonant design frequency goes up, conversely the elements physical size, width and length, must decrease. As the frequency goes up to the 40 GHz upper limit the feed line will actually be wider than some patches (above 30 GHz). Frequency is directly proportional to $W_0$ [26]. As the frequency increases the feed transmission line width, $W_0$ will need to be increased to maintain a consistent $Z_0$. Therefore, it was concluded that in order to maintain as narrow as possible $W_0$, the $Z_0$ and input impedance were to be designed for 100 Ohms. In order to retain a 50 Ohms overall input impedance, and use a single chassis mount connector, two feed lines were combined to form a parallel input impedance of 50 Ohms.

Another interesting challenge for consideration is dispersion. It is preferred for the feed line to simply allow a pathway for the signal to propagate, but not radiate. As the frequency increases, $Z_0$ and $W_0$ will change thus making the transmission line potentially dispersive. The dispersion comes from Hybrid modes, Non TEM [26].

MATLAB was used to automate all primary calculations associated with this design: all the main parameters discussed in chapter 2, such as wavelength, effective permittivity, patch demensions, inset depth, and so on.

It was somewhat difficult to accurately estimate the exact inset depth of the patch's feed line, to achieve 100-Ohm input impedance. MATLAB was used to estimate the inset depth, $y_0$ and $R_{in}$ based on (22). The results were reasonably comparable to the results from ADS Momentum simulation. The parametric sweep feature of ADS function worked for the first few patches, but soon proved to be unreliable and kept hanging.

As a comparison, MATLAB was used to recreate results from the papers [11,21], using the authors data for center frequency, feed width and patch length. The inset depth results

were not the same as the authors had produced. It is possible that some interpolation may have been used, or the authors used the equations for the initial guess, and then simulation software to gain a more accurate inset depth.

### 2.3.2 Modeling and Simulation

Modeling and simulation software is essential to the design process. Computer programs such as MATLAB, Keysight ADS, Comsol Multi-Physics, Ansys HFSS, CTS, and 4NEC are popular computational electromagnetics (CEM) programs that help to simplify and streamline the design process for computer-aided modeling of antennas and microwave circuits. CEM programs can use varying schemes for simulations, such as Method of Moments (MoM), Finite Element Method (FEM), and finite-difference time domain (FDTD) [27, p 93,63]. Essentially, the applications estimate the solutions for Maxwell's equations for the radiating antenna structure. FEM and FDTD focus on the solution to Maxwell's equations in differential form, whereas MoM uses superposition integration and Green's function [27, p 185]. Professionally supported CEM programs are very expensive. Most CEM programs recommend a very fast processor and at least 32 Gbits of RAM. The programs require training and support, therefore, can be challenging to master without the support of the manufacture. Programs considered for this thesis were Comsol Multi-Physics (Comsol) and Keysight ADS (ADS). Comsol is a server based software at WSU, and usually requires local access to the server from a lab computer. Remote access is possible, but can be slower than running the simulation on a local machine. Comsol is very comprehensive and detailed in its setup and was actually preferred over ADS. However, ADS was readily available for remote computer use and does not require the university's central file server; therefore it was used out of convenience.

## 2.4 Summary

Information regarding the background, design criteria and unique characteristics of patch antennas, in addition to the Log Periodic Design Method were presented. The unique properties that lead to ultra wide-band width and a broadside radiation pattern, make the log periodic method the sensible design choice to meet the goals of this research.

The research presented, provides a very straight- forward and reasonable approach to implement the design method. The cited antenna designers all used the same scaling factor of $\tau = 1.05$ and the same transmission line method for estimating the array parameters. The equations presented provide a basic estimate and approach to the design, and therefore lay the foundation for the estimated final design. Of course, simulations in ADS Momentum produce a more precise design. Antenna design cannot be all mathematical and will require some interpretation of the results to get a feel for what works and what does not. Some trial and error comes into play to develop the proper design. Therefore, one could potentially improve on a design by simply studying the problem further and being diligent to optimize the design. However, antenna design can be arduous and often requires expensive test equipment, simulation software, anechoic chambers, network analyzers, post processing software, and so on. For the research presented here, much time has been invested already and there comes a point where trade offs had to be made. For example, during the parametric sweep stage of design simulation, length $d_m$, $I_m$, had to be adjusted to optimize the $VSWR$ or $R_L$. However, this can be very time consuming and therefore best efforts were made to bring an appropriate and acceptable conclusion to the work.

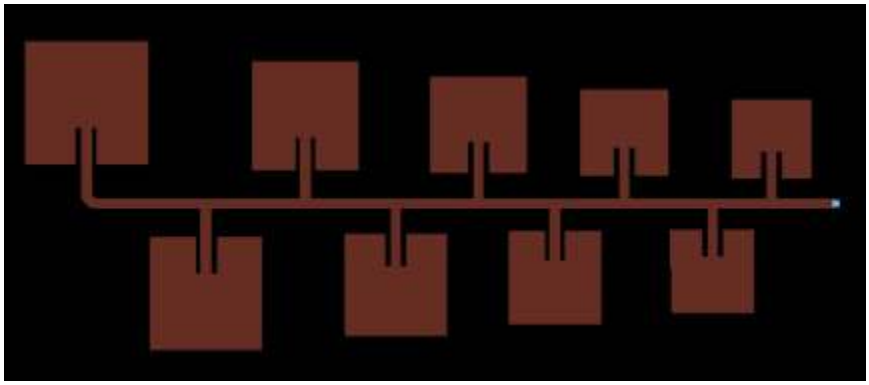

Figure 13: EM layout of 9-element, 2-3GHz LPMSAA, created in ADS.

# 3 Methodology

## 3.1 How to study the problem

The hypothesis states that the designed and fabricated antenna is to provide the necessary, fractional bandwidth to cover 80% to 133 % of 8-40 GHz with one multiple element, inset feed, LPMSAA. In addition, the antenna will also have a 3-dB beamwidth $<$20 degrees, gain $>$ 3 dBi and $VSWR$ $<$1.8 over the entire $BW$.

For the research presented here, modeling, simulation, and finally, actual fabrication of the LPMSAA is preferred. However, due to the lack of resources, only simulation will be used to evaluate the antenna and test the hypothesis.

In order to better understand and verify the design process, a 2-3 GHz LPMSAA was constructed using the methods described in Chapter 2. Since the 2-3 GHz LPMSAA was designed already, it makes sense to design the antenna for practice. The primary design parameters are shown in Table 2 and are similar to [21]. Following initial design, the antenna was laid out and simulated in ADS. The $R_L$, $VSWR$ and 3-D antenna patterns were simulated. The 9-element array is shown in Figure 13. The results from the paraemetric sweep are shown in Figures 14 and 15. The results for this sweep are reasonable, a $R_L$ less than -9.5 dBm and or VSWR less than 2 are the minimum requirements for good resonance. The mesh setting for this example was at 10 cells per wavelength.

Table 2: 2-3 GHz LPMSAA primary parameters.

| Element | $f_0$ | $W = L$ | $I_m$ | $d_m$ | $R_{in}, (50\ Ohms)$ |
|---|---|---|---|---|---|
| Number | (GHz) | (mm) | (mm) | (mm) | (mm) |
| 1 | 2.04 | 33.89 | 19.38 | 35.36 | 10.8 |
| 2 | 2.14 | 32.27 | 18.46 | 32.09 | 10.4 |
| 3 | 2.25 | 30.71 | 17.58 | 61.23 | 9.8 |
| 4 | 2.37 | 29.22 | 16.74 | 55.45 | 9.55 |
| 5 | 2.48 | 27.82 | 15.94 | 50.07 | 9.0 |
| 6 | 2.60 | 26.47 | 15.18 | 45.08 | 8.6 |
| 7 | 2.73 | 25.19 | 14.46 | 40.44 | 8.2 |
| 8 | 2.87 | 23.97 | 13.77 | 36.15 | 7.8 |
| 9 | 3.01 | 22.80 | 13.12 | 27.46 | 7.5 |

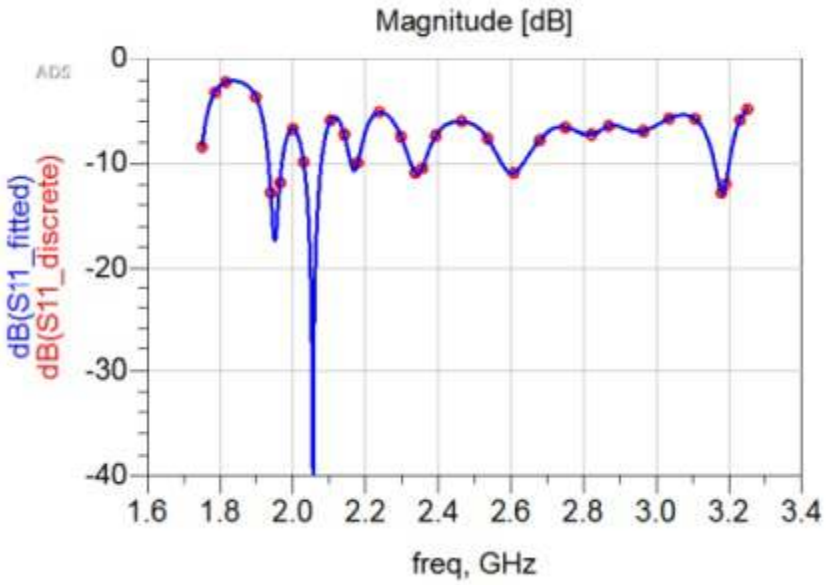


Figure 14: Return loss simulation results for 9-element, 2-3 GHz LPMSAA.

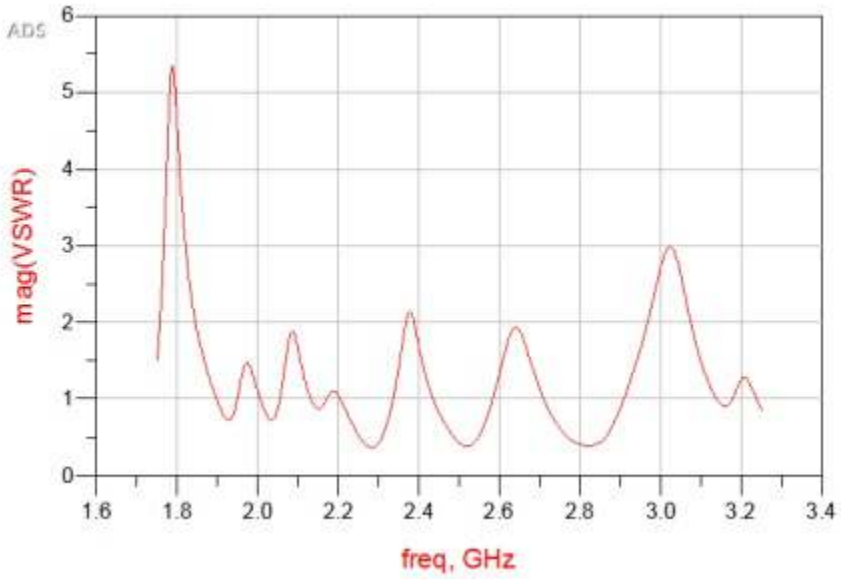


Figure 15: VSWR simulation results for 9-element, 2-3 GHz LPMSAA.

## 3.2 Describe the experiment

For the 8-40 GHz LPMSAA, the design method will follow a similar process, as the aforementioned 2-3 GHz LPMSAA and as shown in chapter 2. However, with a major exception that the results of the experiment will come from simulation only. Some other changes are necessary and one in particular will be the substrate material. The design will be laid out on a low-permittivity substrate, Rogers Duroid 5880, which has a dielectric constant of approximately 2.2 and 1.57 millimeter substrate height. The low-permittivity substrate will allow a wider $BW$ to be attained, per-element, as per (11). Should one compare FR-4 substrate to Rogers Duroid 5880, the $BW$ of the individual patches are expected to increase by a factor of 1.5 times that is, if the other factors are held constant. Another important change will be in the RF connector. Since Sub-miniature A (SMA) connectors are generally not used above 18 GHz then the LPMSAA will use a 2.92 millimeter connector (should actual fabrication occur). 2.92 millimeter connectors are reliable up to about 40 GHz [28]. The primary parameters for the LPMSAA design are shown in Table 3. The data set was used as a starting point and is therefore an estimate into the final design based on the equations

in chapter 2.

## 3.3 Analysis Method

There are various methods that can be used to research and develop our array, namely the Transmission Line or Cavity Models. The transmission line method is a simple method that is not as accurate as the Cavity Model Method, but it is a model that uses transmission line theory, and thus has straight-forward equations that can be used to calculate the approximate width, length, frequency, input resistance, etc. The design parameters can be generated in MATLAB and the schematic can be captured in ADS, or other CEM program. For the work here the schematic layout was modeled in ADS using MOM simulation. The ADS simulation performs an S-parameter sweep. The data display window presents the graphical representation of return loss magnitude and phase versus frequency. The embedded equation editor was used to convert scattering parameters to impedance parameters, $S_{11}$ to $Z_{11}$. The impedance parameters can be calculated as [16, p 192]

$$Z_{in} = Z_0 \frac{1 + S_{11}}{1 - S_{11}}. \tag{41}$$

Markers were used to determine the input impedance $R + jX$ result at the resonant frequency of each patch.

## 3.4 Evaluation of the Results

The antenna will be evaluated for pass or fail results, as per the hypothesis requirements, using the output data from the ADS sweeps. The antenna fractional bandwidth requirement, can be verified by the overall evaluation of the test parameters. The VSWR $<$1.8 requirement shall be evaluated by inspection of the average VSWR plot versus frequency. In order to test the gain and beamwidth, far-field data is required to be collected. The 3-dB beamwidth $<$20 degrees can be verified by inspection of the radiation intensity plots for

Table 3: 8-40 GHz LPMSAA primary parameters.

| Element Number | $f_0$ (GHz) | $W = L$ (mm) | $I_m$ (mm) | $d_m$ (mm) | $R_{in}, (103wq0\ Ohms)$ (mm) |
|---|---|---|---|---|---|
| 1 | 8.0 | 11.75 | 14.39 | 6.25 | 3.8 |
| 2 | 8.4 | 11.13 | 13.7 | 5.89 | 3.6 |
| 3 | 8.82 | 10.56 | 13.05 | 5.55 | 3.42 |
| 4 | 9.26 | 10.0 | 12.42 | 5.22 | 3.25 |
| 5 | 9.72 | 9.47 | 11.83 | 4.91 | 3.08 |
| 6 | 10.21 | 8.96 | 11.27 | 4.6 | 2.92 |
| 7 | 10.72 | 8.48 | 10.73 | 4.33 | 2.77 |
| 8 | 11.26 | 8.03 | 10.22 | 4.06 | 2.63 |
| 9 | 11.82 | 7.6 | 9.74 | 3.81 | 2.5 |
| 10 | 12.41 | 7.18 | 9.27 | 3.56 | 2.36 |
| 11 | 13.03 | 6.78 | 8.83 | 11.28 | 2.24 |
| 12 | 13.68 | 6.4 | 8.41 | 10.33 | 2.12 |
| 13 | 14.37 | 6.05 | 8.01 | 9.43 | 2.0 |
| 14 | 15.1 | 5.71 | 7.63 | 8.6 | 1.9 |
| 15 | 15.84 | 5.38 | 7.27 | 7.8 | 1.8 |
| 16 | 16.63 | 5.08 | 6.92 | 7.39 | 1.7 |
| 17 | 17.46 | 4.71 | 6.6 | 1.29 | 1.59 |
| 18 | 18.34 | 4.43 | 6.59 | 4.83 | 1.5 |
| 19 | 19.25 | 4.24 | 6.92 | 1.79 | 1.44 |
| 20 | 20.22 | 3.98 | 7.26 | 1.03 | 1.36 |
| 21 | 21.22 | 3.74 | 7.63 | 5.86 | 1.28 |
| 22 | 22.29 | 3.51 | 8.0 | 5.0 | 1.21 |
| 23 | 23.4 | 3.3 | 8.41 | 4.21 | 1.14 |
| 24 | 24.57 | 3.09 | 8.82 | 3.48 | 1.08 |
| 25 | 25.8 | 2.9 | 9.27 | 2.79 | 1.01 |
| 26 | 27.09 | 2.72 | 9.73 | 2.15 | 0.95 |
| 27 | 28.44 | 2.54 | 10.22 | 1.56 | 0.89 |
| 28 | 29.87 | 2.38 | 10.73 | 1.01 | 0.85 |
| 29 | 31.36 | 2.22 | 11.27 | 4.07 | 0.8 |
| 30 | 32.92 | 2.08 | 11.83 | 3.27 | 0.75 |
| 31 | 34.58 | 1.94 | 12.42 | 2.52 | 0.7 |
| 32 | 36.3 | 1.8 | 13.05 | 1.83 | 0.66 |
| 33 | 38.12 | 1.68 | 13.7 | 1.18 | 0.62 |

10, 20, 30, and 40 GHz 2-D slices of XZ, YZ and XY planes. The half-power beamwidth is the angle, in degrees, between the two half power points on the radiation pattern cut that contains the maximum lobe [25]. The main lobe width will be inspected at the half-power point. The antenna gain can be verified to be $> 3$ dBi by inspection of the gain plots versus frequency.

## 3.5 Summary

It is suggested, to first design the antenna using the equations in chapter 2 and then use the data to create a layout in ADS or a similar CEM program. Since the LPMSAA will be simulated and not fabricated ADS is a good choice to perform the sweeps and evaluate the far-field data. Once the sweeps and far-field data are collected, one can complete the evaluation of the results and compare to the hypothesis. The evaluation of the results and pass fail criteria can be easily determined by using the plots that are available in ADS.

# 4 LPMSAA Design and Simulation Results

This experiment was reviewed, and evaluated by theoretical analysis only. Matlab was used to create the necessary design parameters and the simulation was done with ADS.

## 4.1 Engineered Drawing

Using the design parameters as shown in Table 3 the 8-40 GHz LPMSAA was laid out in ADS. The antenna is 219 mm long x 60 mm wide. An engineered drawing of the antenna is shown in Figure 16.

## 4.2 ADS Simulation Sweeps

Since 8-40 GHz is such a wide bandwidth ADS had problems running the simulation in one sweep. Therefore, the sweeps were broken into three, 50-point adaptive sweeps: 8-20

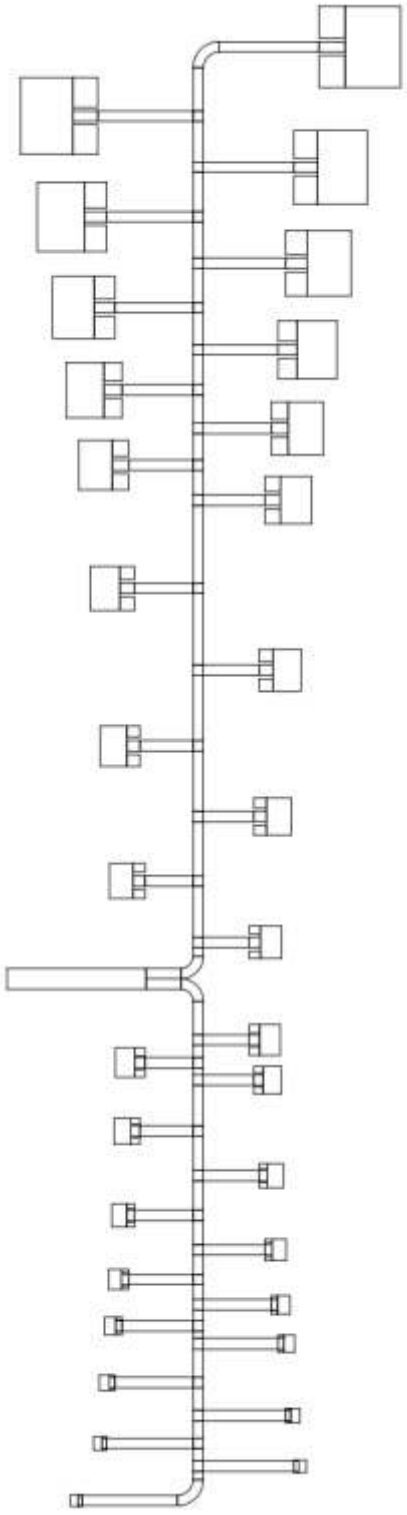

Figure 16: Engineered drawing of LPMSAA.

Table 4: 8-40 GHz LPMSAA radar band performance.

| Band Designator | $f_0$ (GHz) | AVG. $VSWR$ | AVG. $R_L$ (dB) | AVG. $Z_{in}$ Real (Ohms) | AVG. $Z_{in}$ Imaginary (Ohms) |
|---|---|---|---|---|---|
| X | 8-12 | 1.8 | -5 | 100 | -25 |
| Ku | 12-18 | 2.5 | -5 | 125 | -10 |
| K | 18-27 | 3 | -7 | 125 | -75 |
| Ka | 24-40 | 1.75 | -3.5 | 75 | 0 |

GHz, 20-30 GHz and 30-40 GHz. The adaptive sweeps created about 1350 data points of $S11$ data. Many of the graphs are screen shots from ADS. The $R_L$ is the only combined graph plotted outside of ADS.

## 4.3 Return Loss, VSWR, Input Impedance

The $R_L$ and $VSWR$ graphs show the bandwidth of the antenna in Figures 17, 18,19, and 20. A $VSWR < 1.8$ is the requirement acceptable for resonance and a 80% to 133 % bandwidth would be approximately 25.6-42.56 GHz. Upon inspection of the $VSWR$ plots the fractional combined bandwidth is approximately 22 GHz. The $VSWR < 1.8$ at 8-17 GHz, 24.5-25.5 GHz, 27-30 GHz, 30-32.5 GHz, and 33.5-40 GHz. The $R_L$ plot shows fractional resonance from 8-34 GHz.

The input impedance, $Z_{in}$, varies over the entire pass band and is shown in Figures 21, 22, and 23. $Z_{in}$ is referenced to $Z_0$ of 50 Ohms. A summary of the $S_{11}$ data is shown in Table 4.

## 4.4 Far Field Data

### 4.4.1 Half Power Beamwidth

Upon inspection the 3-dB beamwidth ($HPBW$) is greater than 20 degrees for 10 GHz XZ and YZ 2-dimensional slices only. For all other planes the $HPBW \leq 20$ degrees. The radiation intensity is shown in units of Watts per sterad and has a direction associated. The

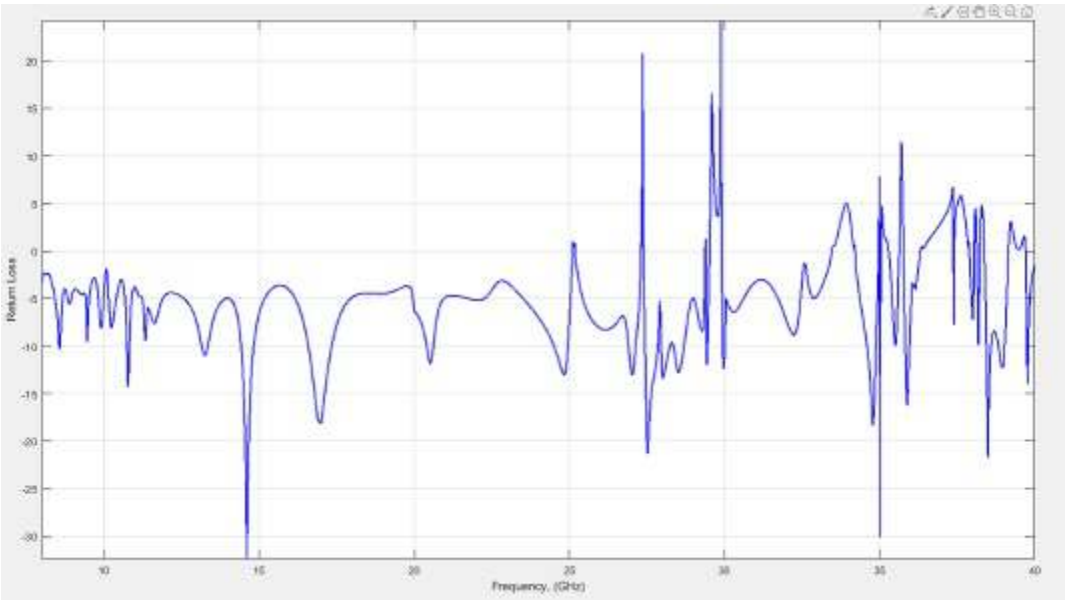


Figure 17: 8-40 GHz LPMSAA Return Loss Magnitude.

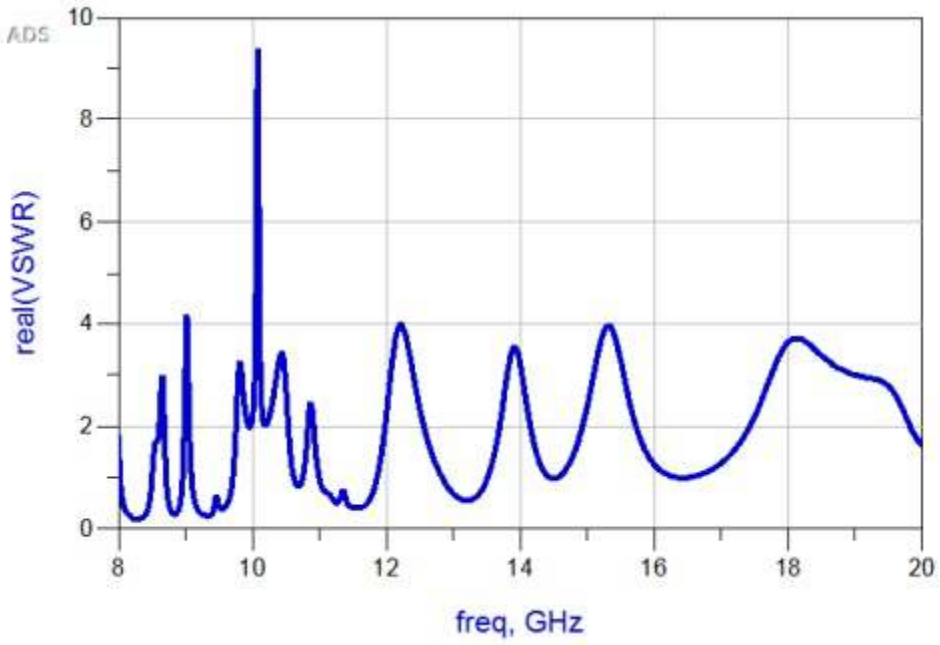


Figure 18: 8-20 GHz LPMSAA VSWR.


Figure 19: 20-30 GHz LPMSAA VSWR.

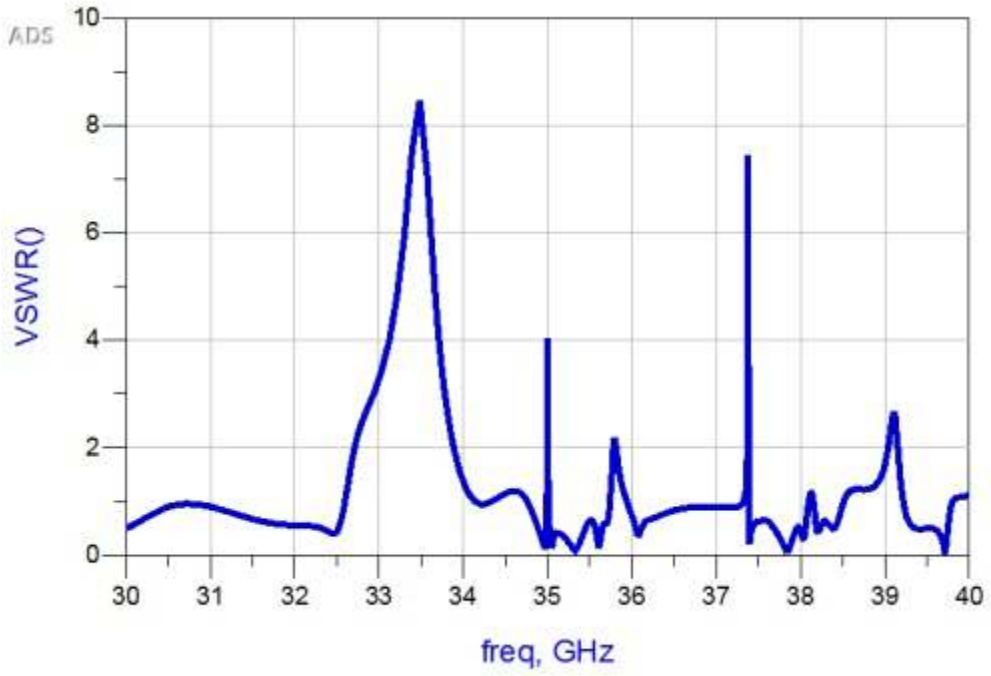


Figure 20: 30-40 GHz LPMSAA VSWR.

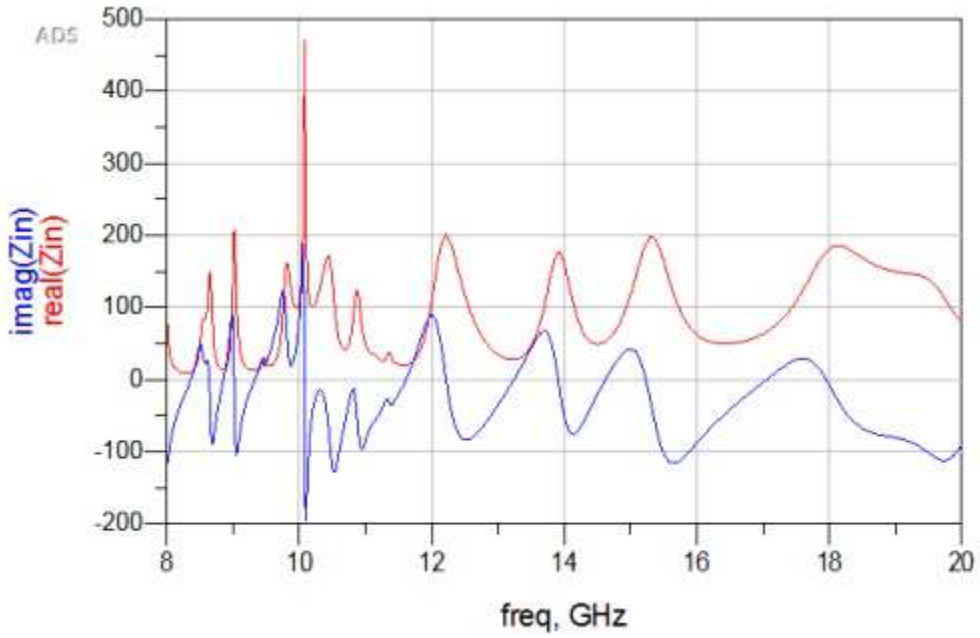


Figure 21: LPMSAA, 8-20 GHz input impedance versus frequency.

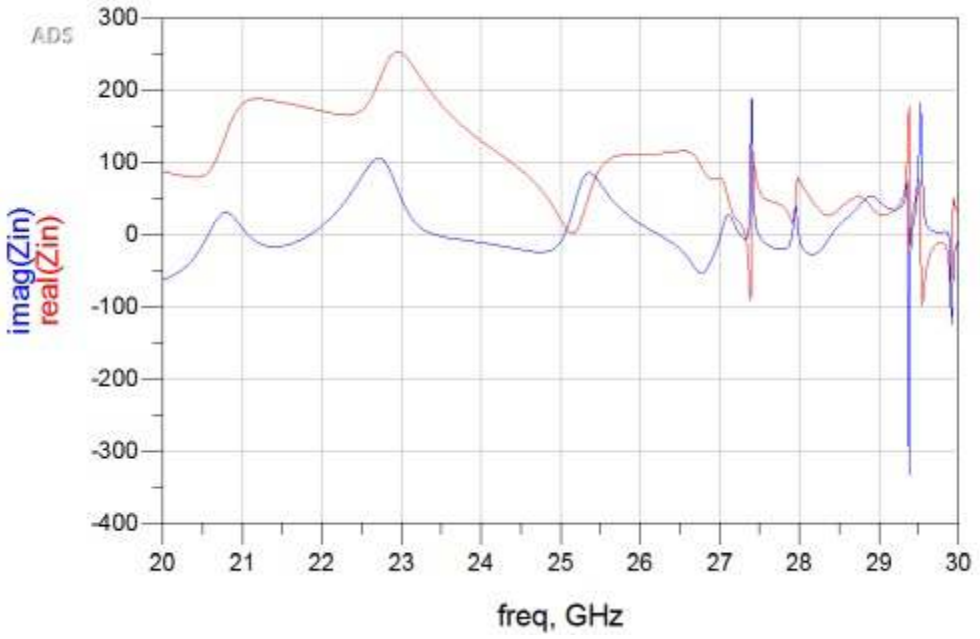


Figure 22: LPMSAA, 20-30 GHz input impedance versus frequency.

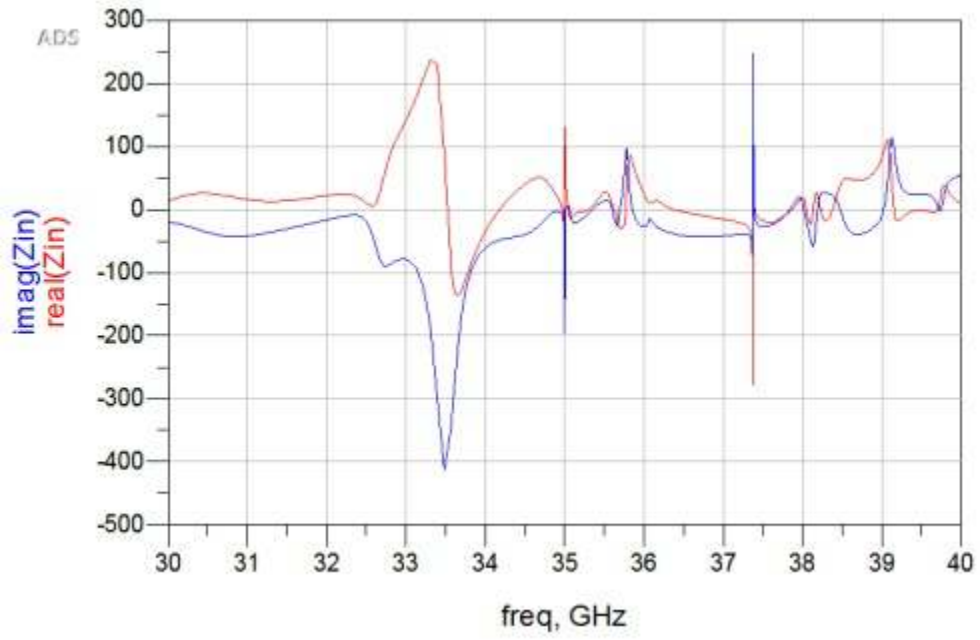


Figure 23: LPMSAA, 30-40 GHz input impedance versus frequency.

radiation intensity is defined as: "In a given direction, the power radiated from an antenna per unit solid angle" [25, p 30]. See Figures 24, 26, 28, 30, 32, 34, 36, and 38 for the radiation intensity plots. Nearly all the radiation power is in the elevation planes, therefore the XY (azimuth) plots are negligible, and are not shown. See Table 5 for detailed $HPBW$ magnitude and angle data.

Table 5: LPMSAA half-power beamwidth.

| $f_0$ | 2-D slice | $HPBW$ | $HPBW$ | offset angle |
|---|---|---|---|---|
| (GHz) | plane | (degrees) | (mWatts) | (degrees) |
| 10 | XZ | 30 | 2 | +35 |
| 10 | YZ | 25 | 2 | +23 |
| 20 | XZ | 15 | 0.55 | +40 |
| 20 | YZ | 15 | 0.3 | +48 |
| 30 | XZ | 20 | 8 | +35 |
| 30 | YZ | 2 | 14 | +1 |
| 40 | XZ | 13 | 72 | -35 |
| 40 | YZ | 10 | 50 | -19 |

Table 6: Far-field electric and magnetic field phasor data.

| $f_0$ | 2-D slice | $\vec{E}_\theta$/angle | $\vec{E}_\phi$/angle | $\vec{H}_\theta$/angle | $\vec{H}_\phi$/angle |
|---|---|---|---|---|---|
| (GHz) | plane | (V/degrees) | (V/degrees) | (mA/degrees) | (mA/degrees) |
| 10 | XZ | 0.5/35 | 0.1/35 | 0.1/35 | 1.5/35 |
| 10 | YZ | 0.25/-55 | 0.55/23 | 1.4/23 | 0.7/35 |
| 20 | XZ | 0.65/40 | 0.1/45 | 0.25/45 | 1.7/40 |
| 20 | YZ | 0.35/-40 | 0.55/-20 | 1.5/45 | 0.8/-40 |
| 30 | XZ | 2.8/-20 | 3.4/-40 | 9/-40 | 7.5/-15 |
| 30 | YZ | 2.8/2 | 2.4/24 | 6/-24 | 8/1 |
| 40 | XZ | 6.7/44 | 6.2/30 | 17/30 | 18/45 |
| 40 | YZ | 8.6/-38 | 7.3/3 | 23/-38 | 19/3 |

Table 7: LPMSAA gain, directivity, and efficiency data.

| $f_0$ | Max Gain | Min. Gain | Max | Efficiency |
|---|---|---|---|---|
| (GHz) | (dBi) | (dBi) | directivity | (percentage) |
| 8-20 | 6.96 | 5.5 | 10.38 | 67 |
| 20-30 | 13.7 | 8.5 | 13.7 | 100 |
| 30-40 | 13.1 | 11 | 13.1 | 100 |

### 4.4.2 Electric and Magnetic Phasor Data

Clearly, the antenna has a broadside radiation pattern. The far-field electric and magnetic field phasor vectors are $\vec{E}_\theta$, $\vec{E}_\phi$, $\vec{H}_\theta$, and $\vec{H}_\phi$. The magnitude and angle are shown in Table 6. The electric and magnetic field patterns are shown in Figures 25, 27, 29, 31, 33, 35, 37, and 39.

### 4.4.3 Gain, Directivity and Efficiency

Clearly, the antenna minimum gain is greater than 3 dB, for the entire pass-band. The minimum gain is 5.5 dB, see Table 7 for a summary of the gain, directivity, and efficiency data. Furthermore, the antenna has an unexpected high efficiency for the 20-30 GHz pass-band.

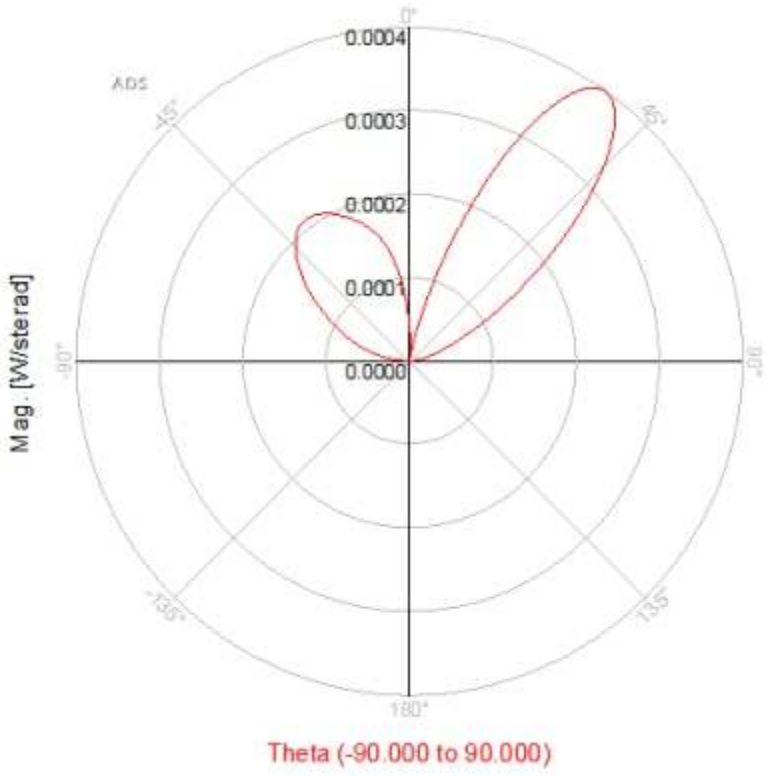


Figure 24: 10 GHz XZ plane far-field radiation intensity.

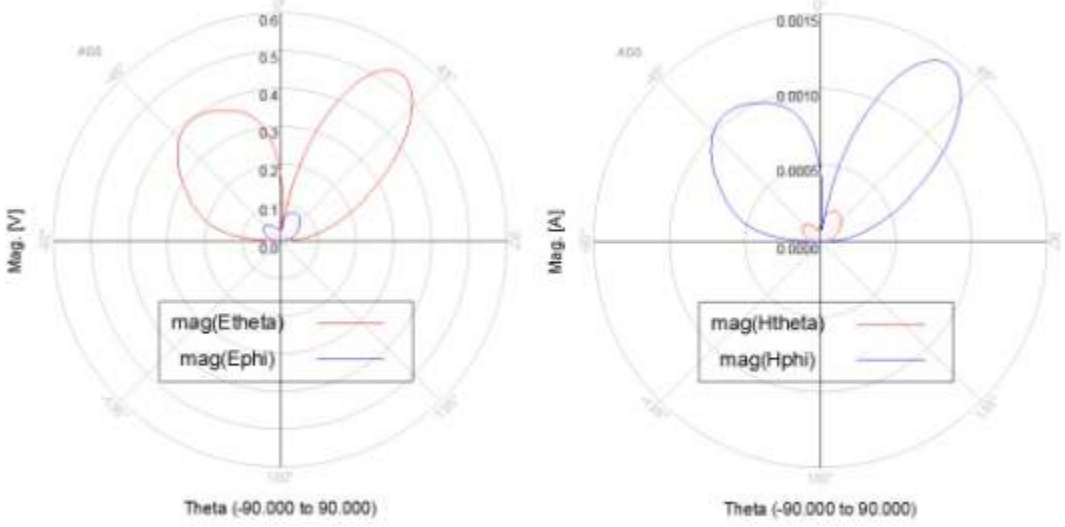


Figure 25: 10 GHz XZ plane electric and magnetic far-field patterns.

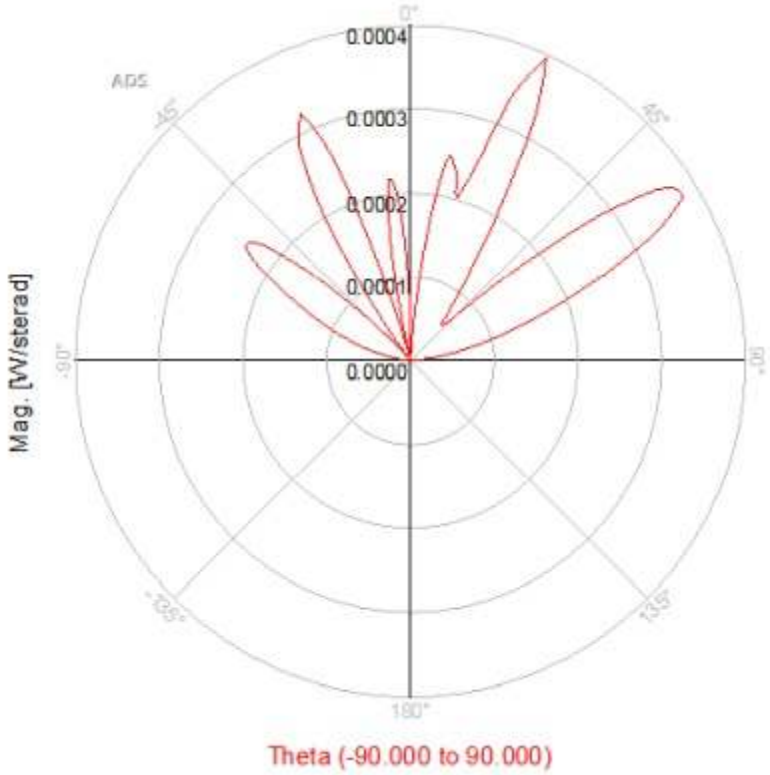


Figure 26: 10 GHz YZ plane far-field radiation intensity.

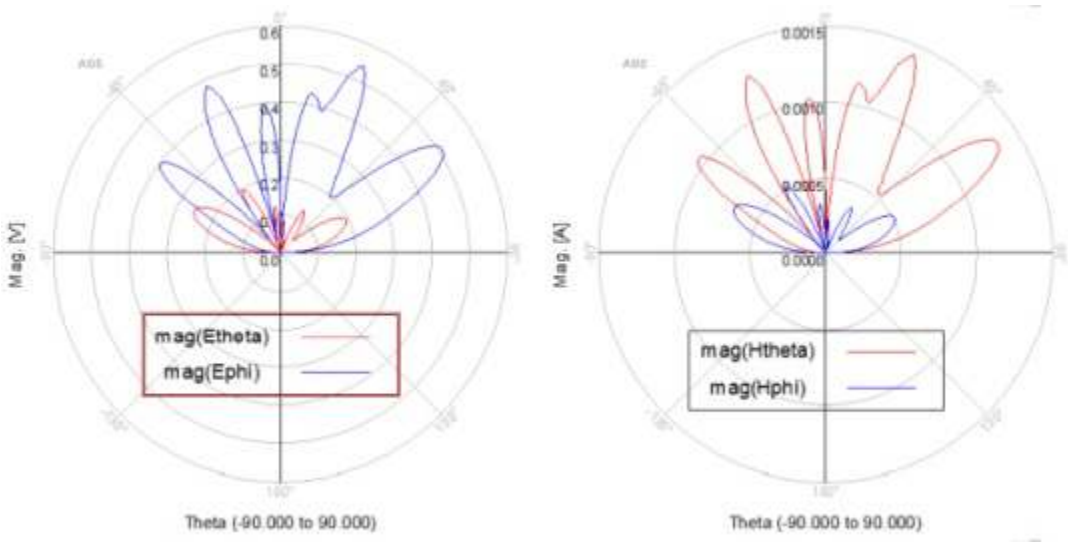


Figure 27: 10 GHz YZ plane electric and magnetic far-field patterns.

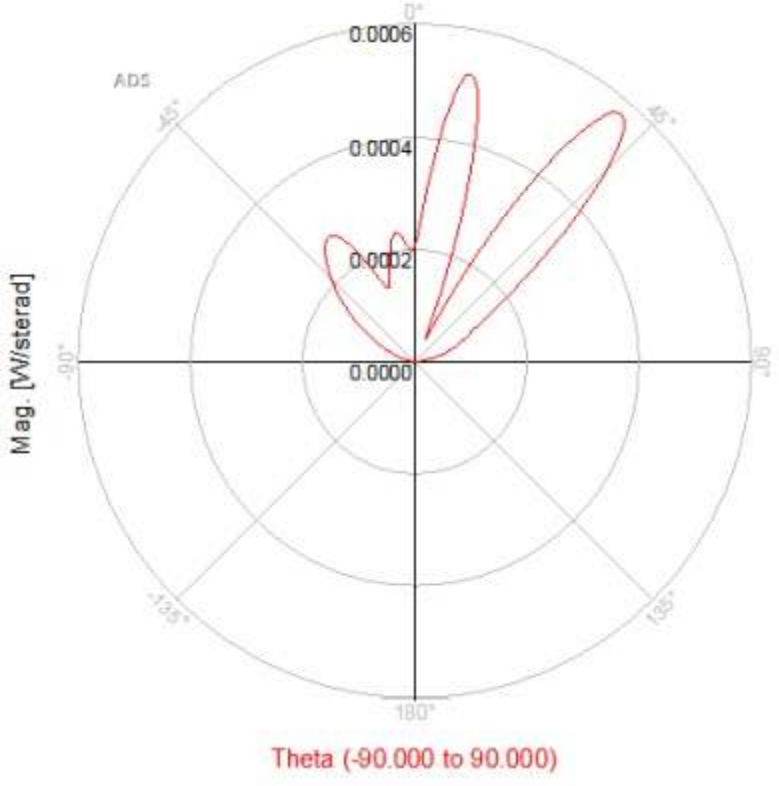


Figure 28: 20 GHz XZ plane far-field radiation intensity.

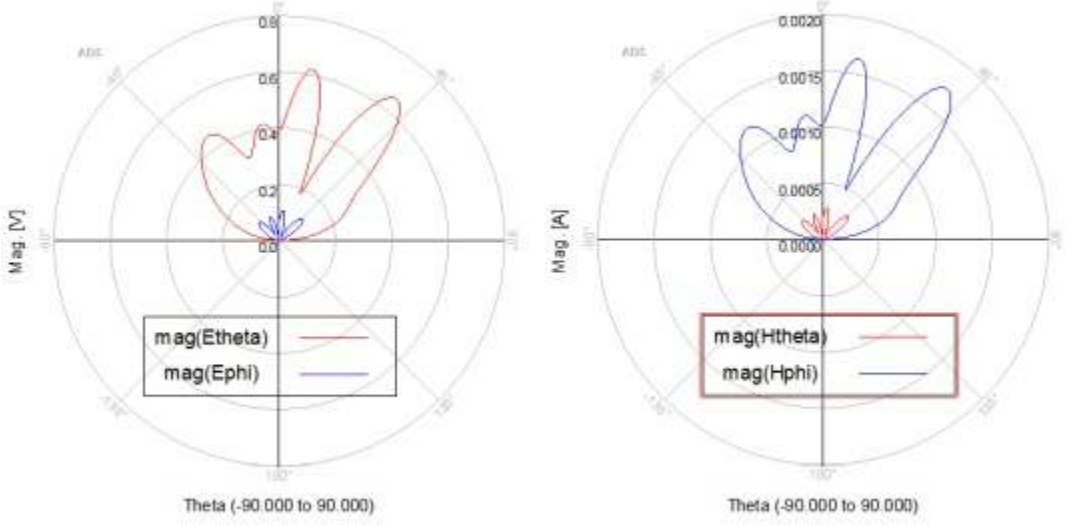


Figure 29: 20 GHz XZ plane electric and magnetic far-field patterns.

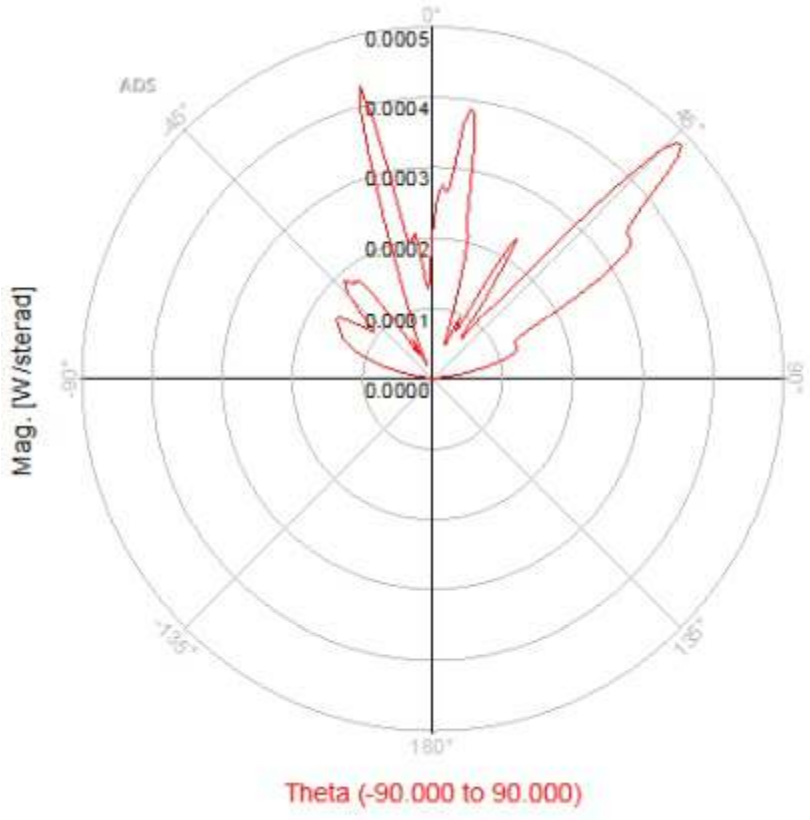


Figure 30: 20 GHz YZ plane far-field radiation intensity.

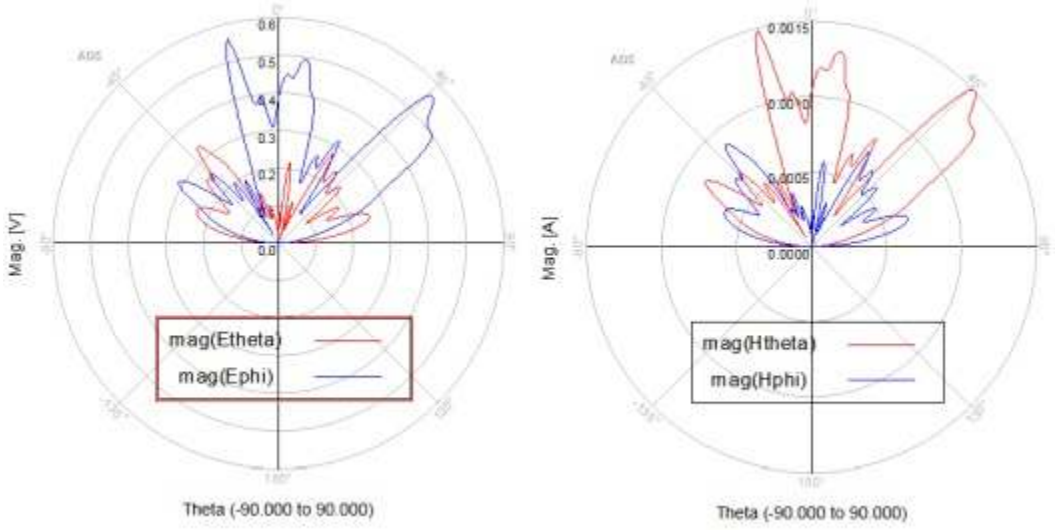


Figure 31: 20 GHz YZ plane electric and magnetic far-field patterns.

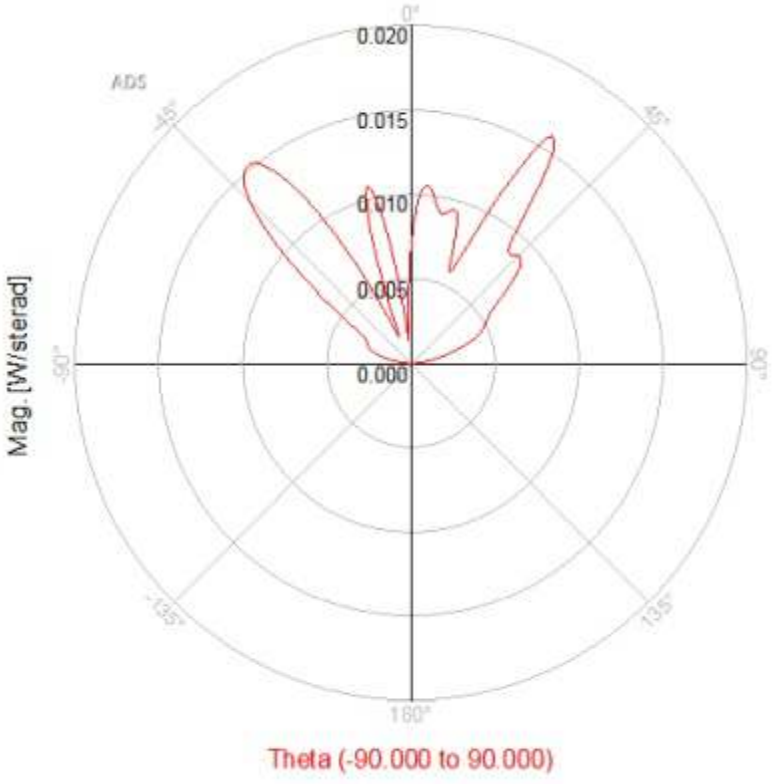


Figure 32: 30 GHz XZ plane far-field radiation intensity.

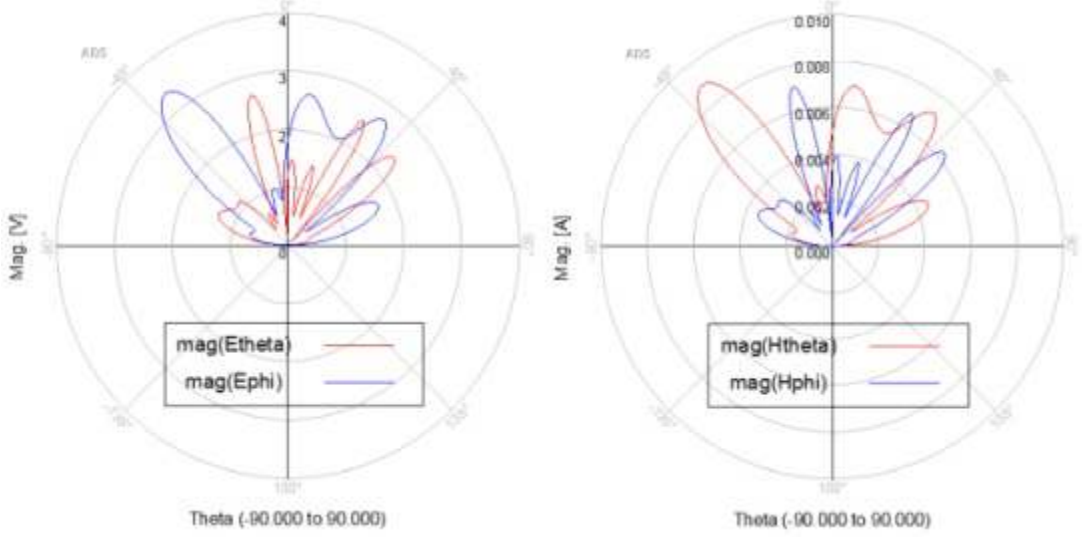


Figure 33: 30 GHz XZ plane electric and magnetic far-field patterns.

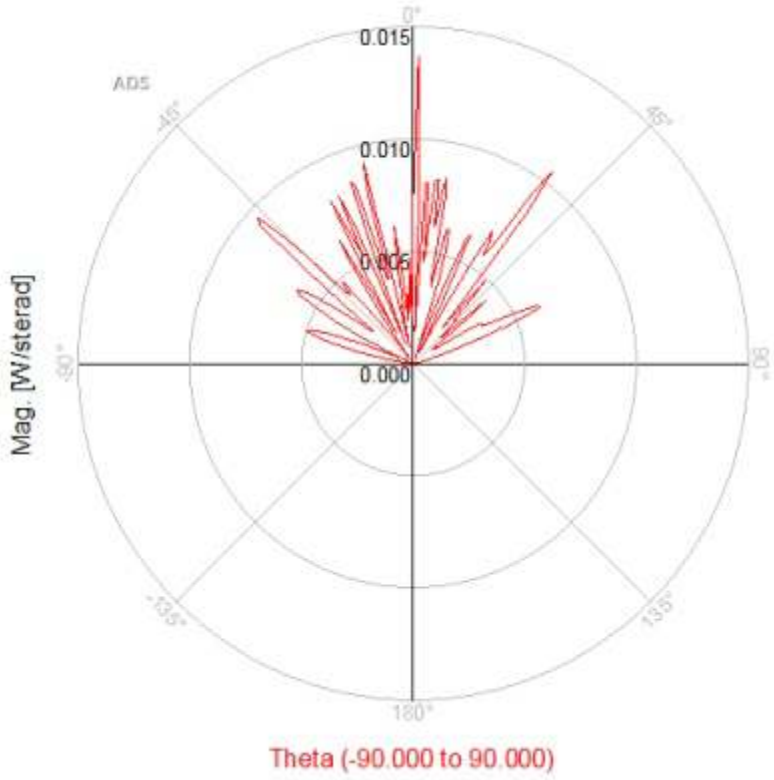


Figure 34: 30 GHz YZ plane far-field radiation intensity.

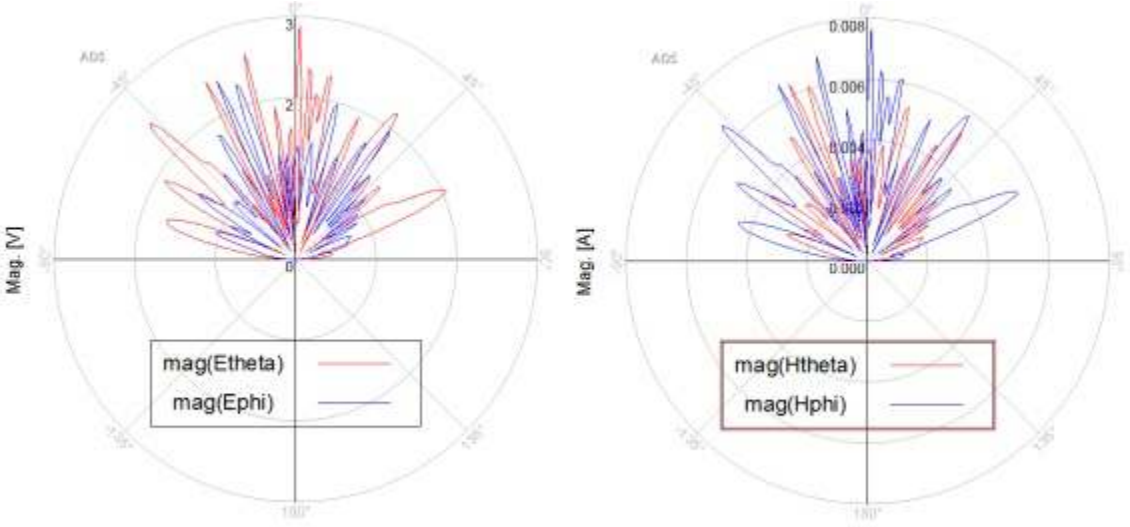


Figure 35: 30 GHz YZ plane electric and magnetic far-field patterns.

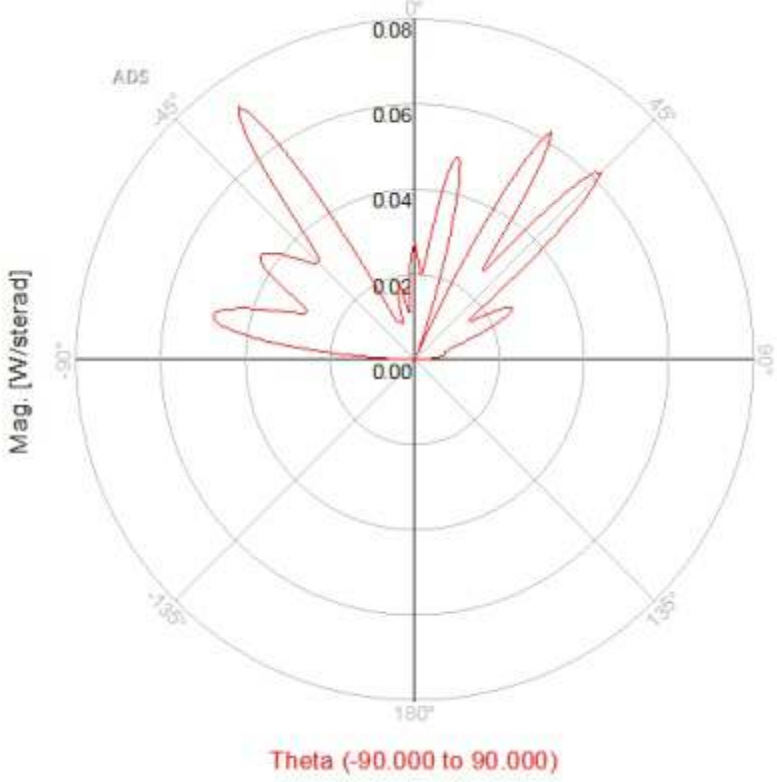


Figure 36: 40 GHz XZ plane far-field radiation intensity.

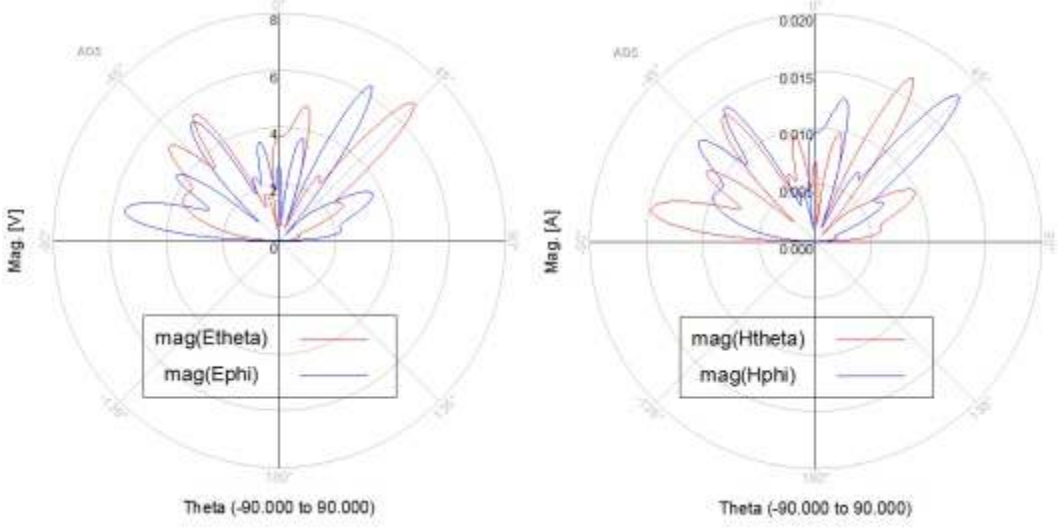


Figure 37: 40 GHz XZ plane electric and magnetic far-field patterns.

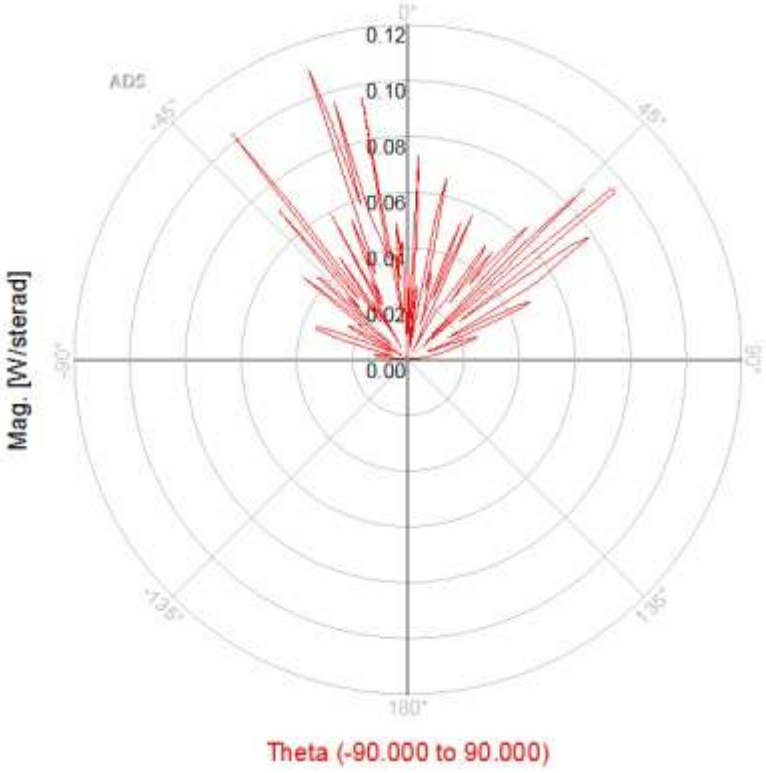


Figure 38: 40 GHz YZ plane far-field radiation intensity.

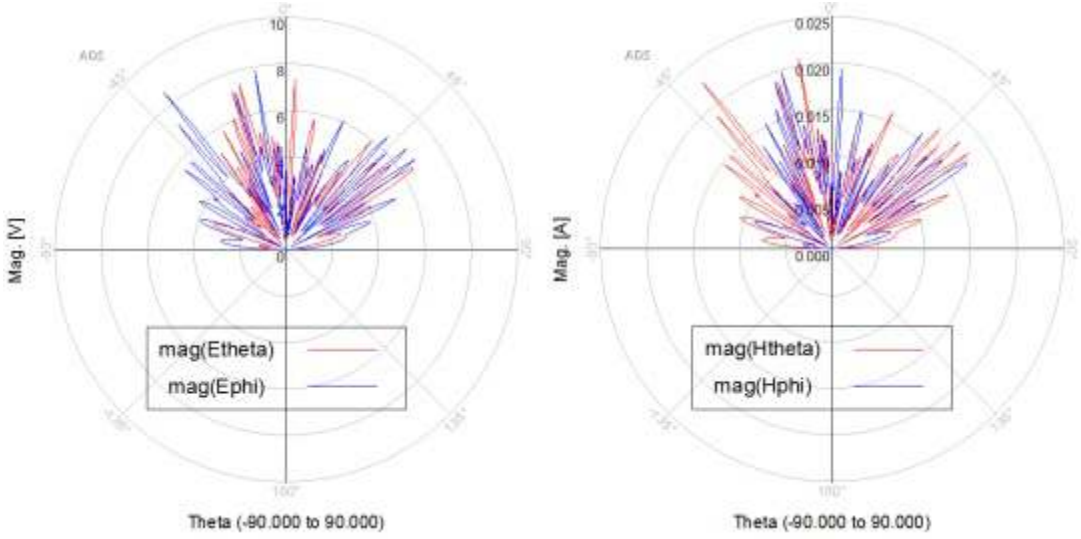


Figure 39: 40 GHz YZ plane electric and magnetic far-field patterns.

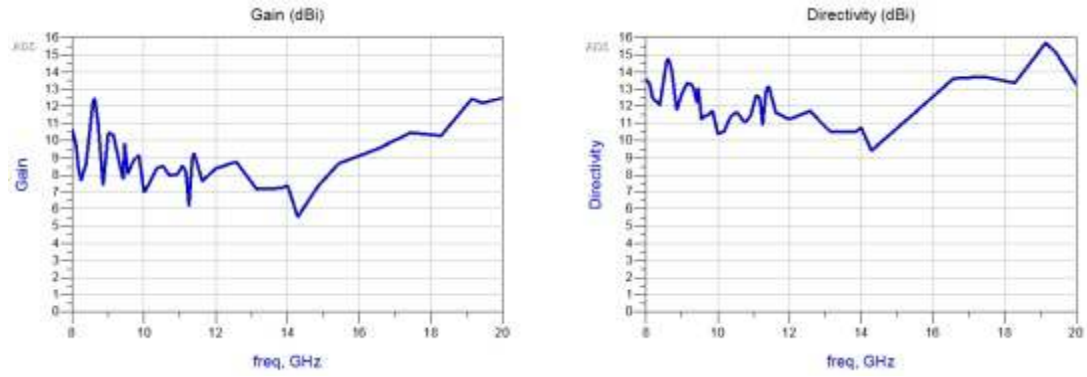


Figure 40: 8-20 GHz gain and directivity versus frequency.

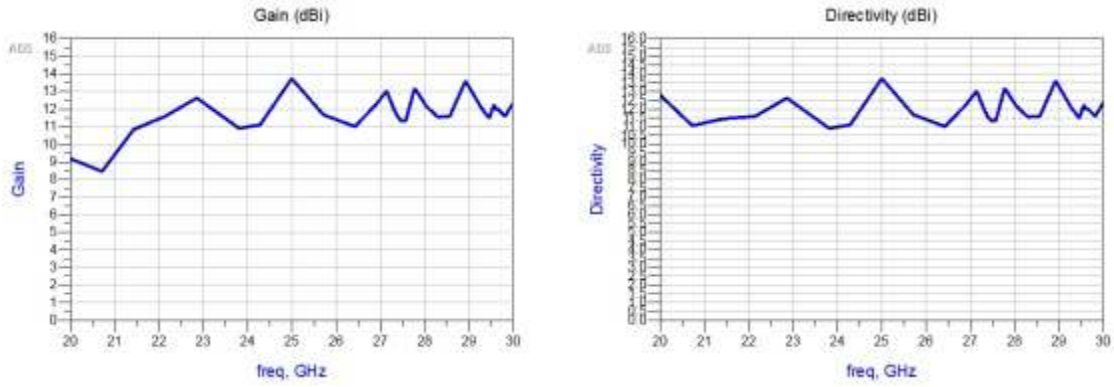


Figure 41: 20-30 GHz gain and directivity versus frequency.

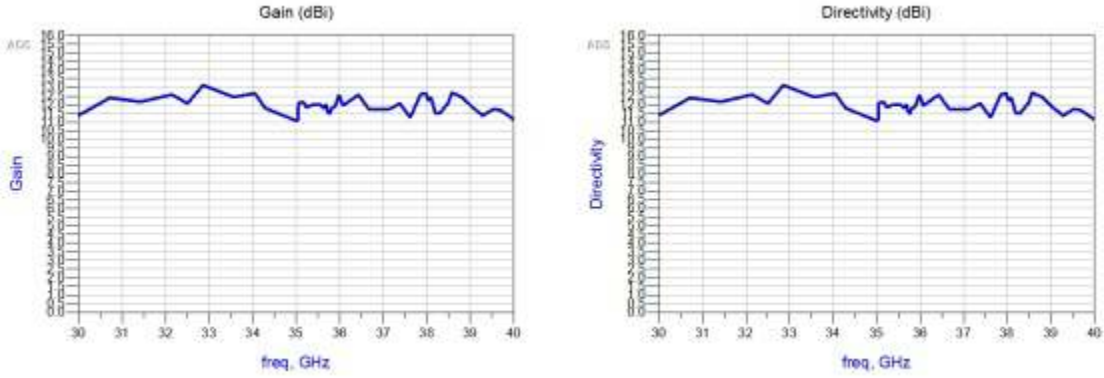


Figure 42: 30-40 GHz gain and directivity versus frequency.

Table 8: Average $\vec{E}$ co to cross polarization data.

| | | Average | Average | |
|---|---|---|---|---|
| $f_0$ | 2-D slice | $\vec{E}$ co pol | $\vec{E}$ cross pol | Isolation |
| (GHz) | plane | (dB) | (dB) | (dB) |
| 10 | XZ | 10 | -30 | 20 |
| 10 | YZ | -10 | -30 | 20 |
| 20 | XZ | -10 | -30 | 20 |
| 20 | YZ | -10 | -25 | 15 |
| 30 | XZ | 10 | -10 | 20 |
| 30 | YZ | 5 | -10 | 15 |
| 40 | XZ | 10 | 0 | 10 |
| 40 | YZ | 15 | 0 | 15 |

### 4.4.4 Co and Cross pol Isolation

The LPMSAA co to cross polarization isolation graphs are shown in Figures 43, 44, 45, 46, 47, 48, 49, and 50. The preferred polarization being the co-polarization and the $90$ degree offset is called cross-polarization. The graphs show good isolation between the polarization slices up to 20 dB for 10 GHz through 30 GHz. From 30 GHz to 40 GHz isolation is lower and ranges 10 dB to 15 dB. Table 8 shows a summary of the co to cross polarization data.

### 4.4.5 Antenna Polarization

Microstrip patch array's are expected to have either linear or circular polarization, [4, p. 813]. However, no antenna is expected to possess perfect polarization dominance. The post processing module of ADS has an "antenna parameters" display window that shows the primary parameters for overall maximum data. The antenna parameters feature does not include the 2-D slice data, but only specific frequency data. A screen shot of the window is shown in Figure 51. The $\vec{E}_\theta$ and $\vec{E}_\phi$ magnitude and phase data can be used to help determine the electric field polarization. The far-field phasor vector is described as

$$\tilde{\mathbf{E}} = \vec{E}_\theta \hat{\theta} + \vec{E}_\phi \hat{\phi}. \tag{42}$$

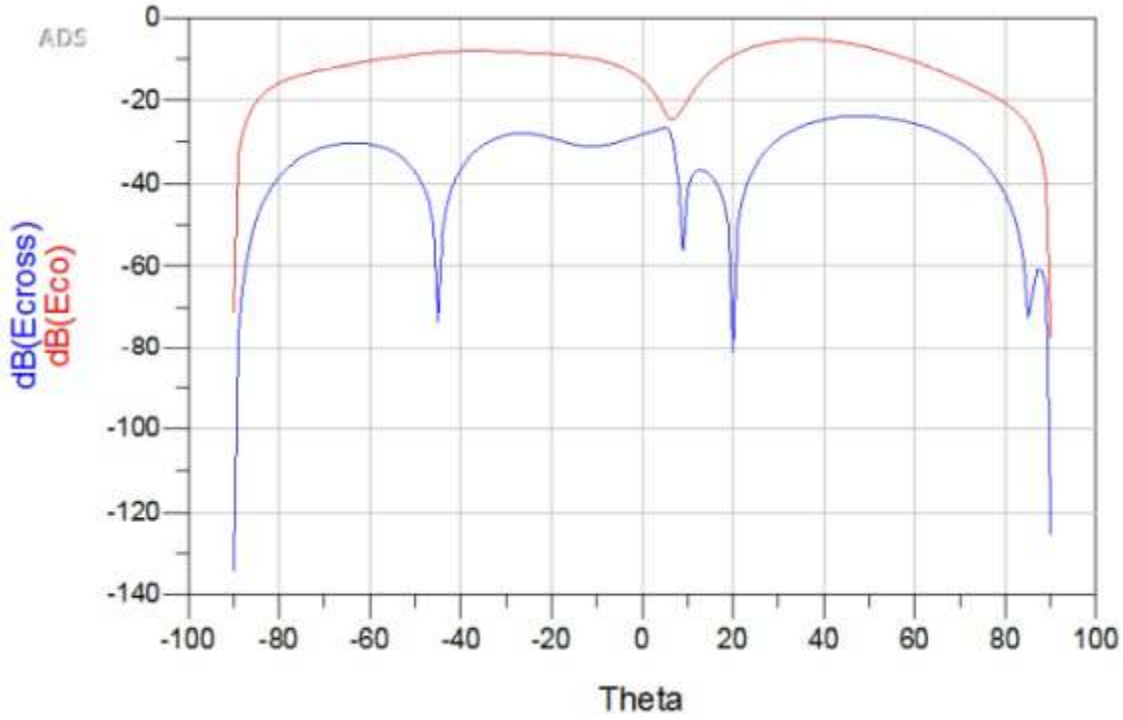


Figure 43: LPMSAA, 10 GHz, XZ plane, $\vec{E}$ co versus cross pol.

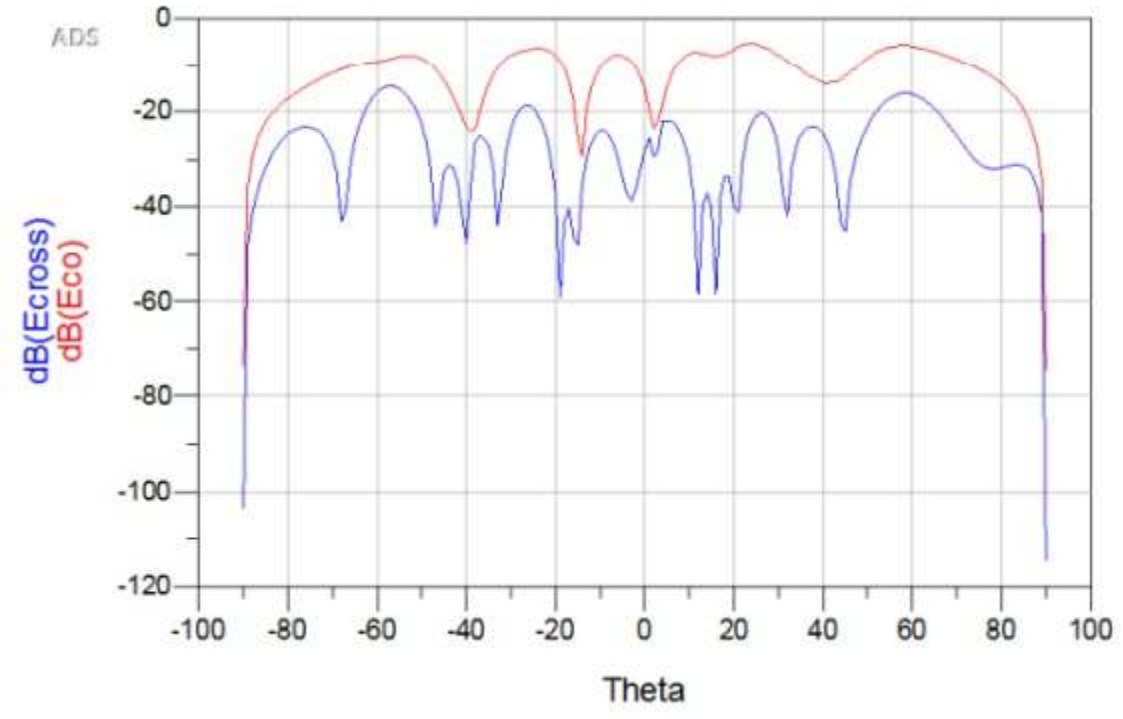


Figure 44: LPMSAA, 10 GHz, YZ plane, $\vec{E}$ co versus cross pol.

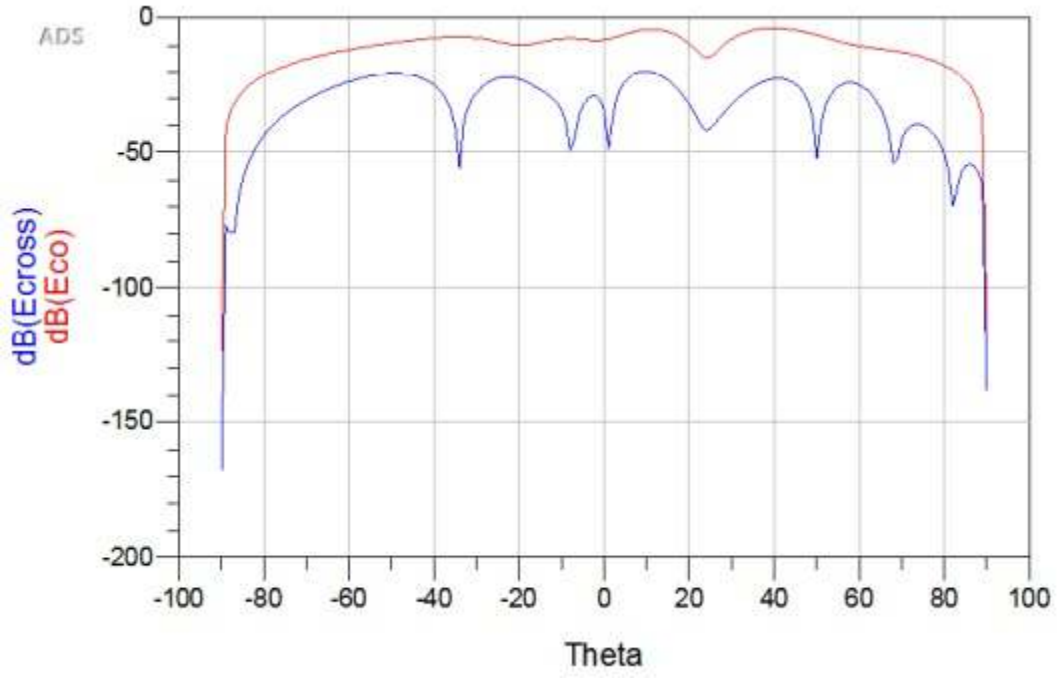


Figure 45: LPMSAA, 20 GHz, XZ plane, $\vec{E}$ co versus cross pol.

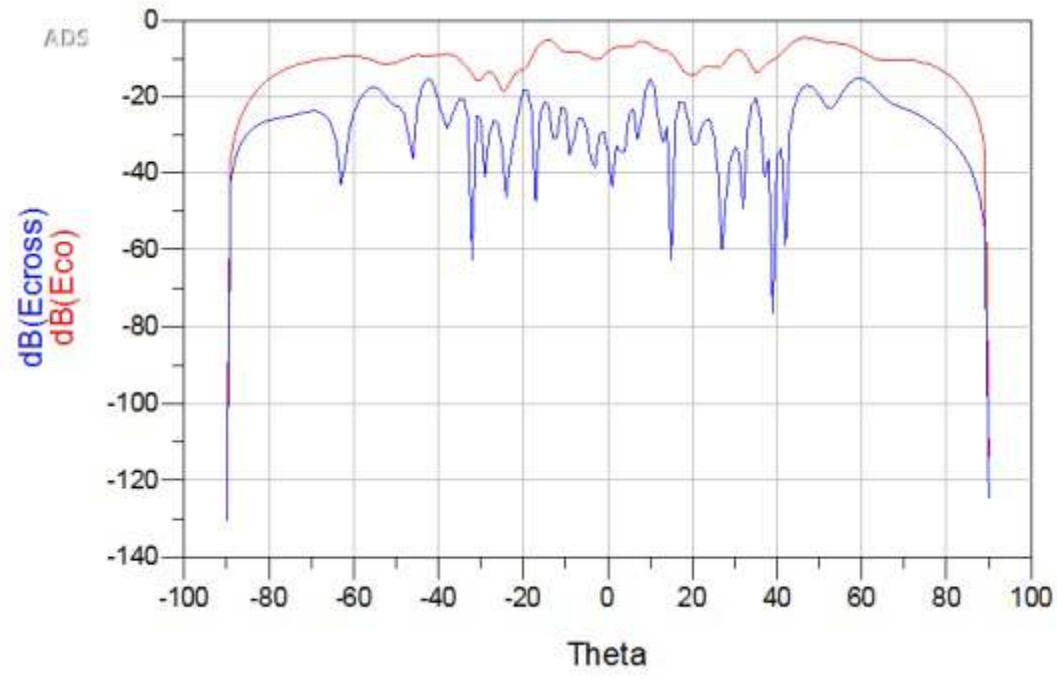


Figure 46: LPMSAA, 20 GHz, YZ plane, $\vec{E}$ co versus cross pol.

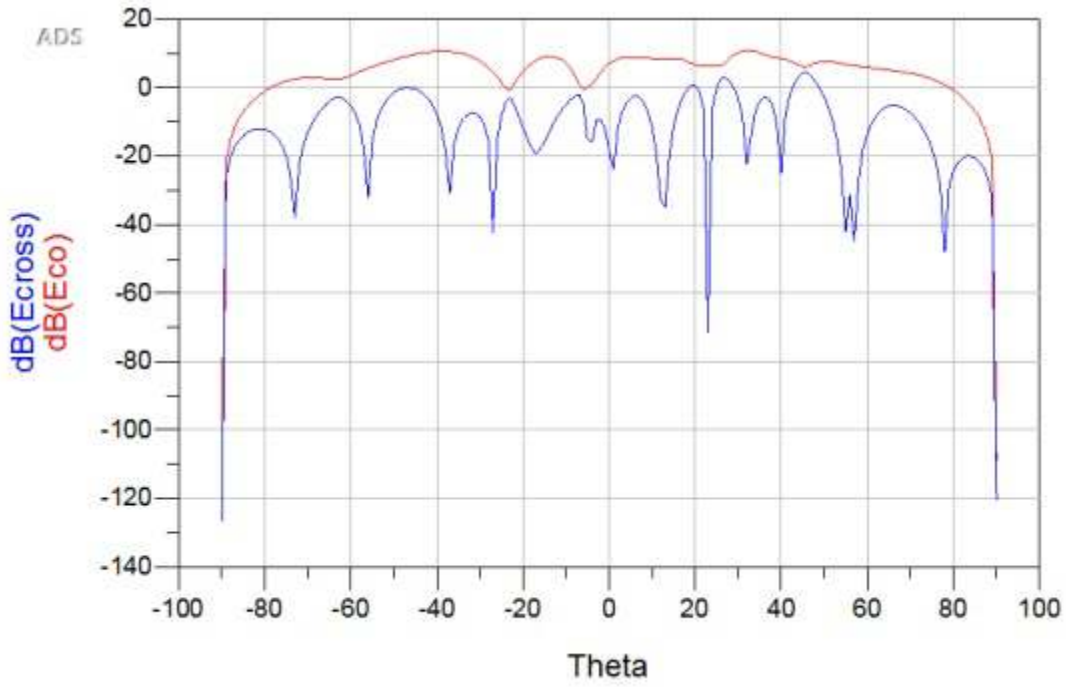


Figure 47: LPMSAA, 30 GHz, XZ plane, $\vec{E}$ co versus cross pol.

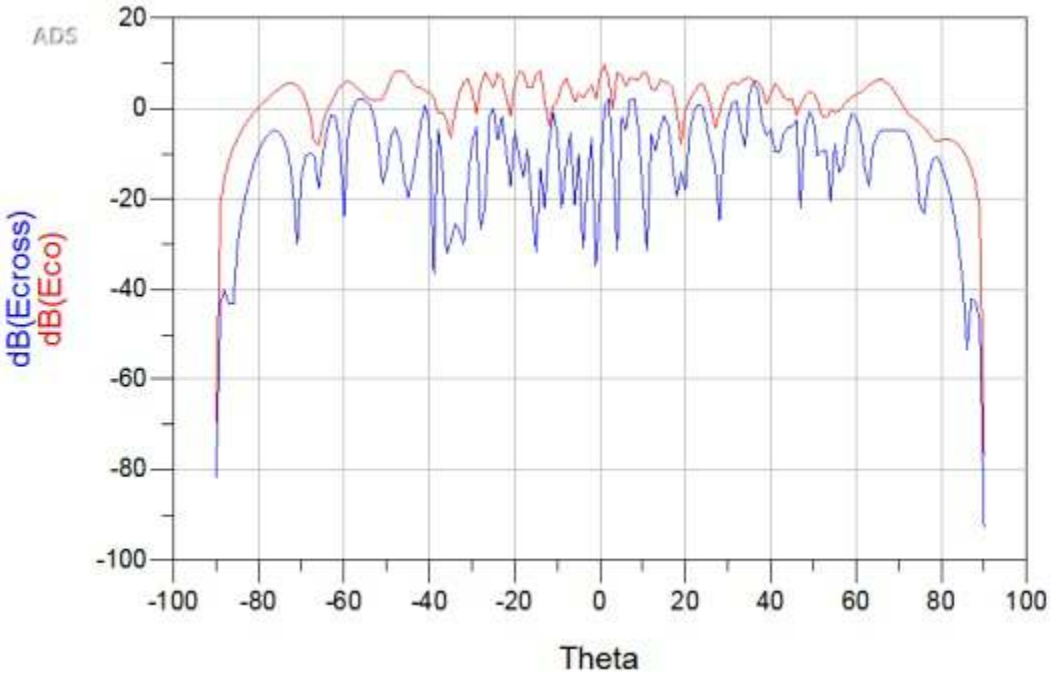


Figure 48: LPMSAA, 30 GHz, YZ plane, $\vec{E}$ co versus cross pol.

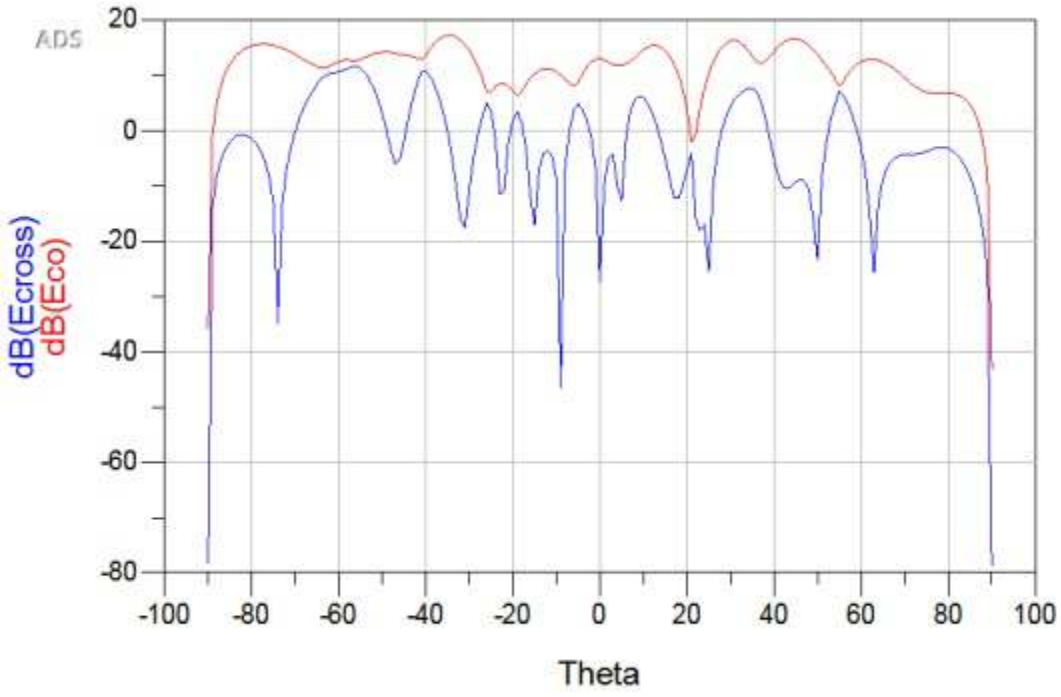


Figure 49: LPMSAA, 40 GHz, XZ plane, $\vec{E}$ co versus cross pol.

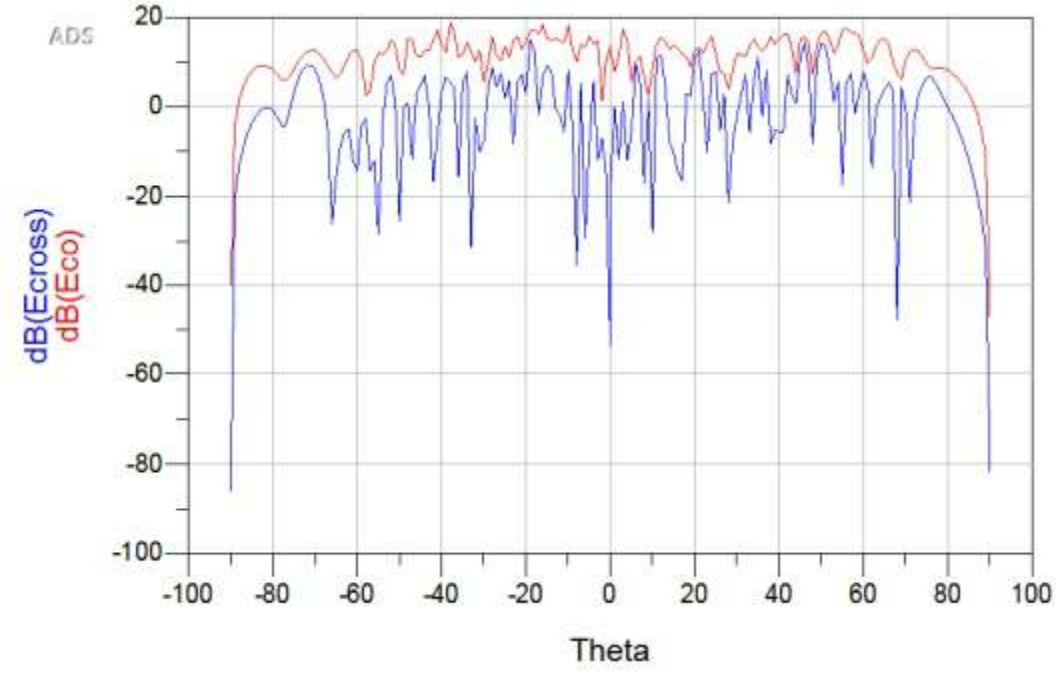


Figure 50: LPMSAA, 40 GHz, YZ plane, $\vec{E}$ co versus cross pol.

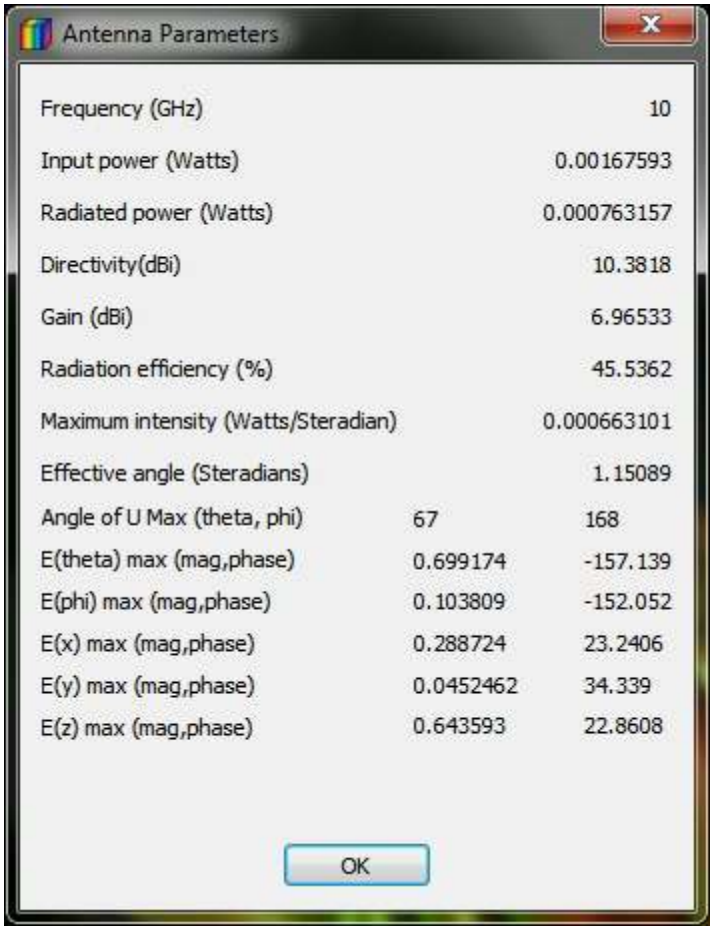


Figure 51: 10 GHz, antenna parameters screen shot.

The difference in phase between the $\vec{E}_\theta$, $\vec{E}_\phi$ and the magnitude of each can be seen in the figure. The constraints are as follows: if the phase difference is equal to $0$ or $n\pi$, then the antenna is said to be linearly polarized. If the phase difference is $\frac{\pi}{2}$ and the magnitudes of the phasor vector's are equal, then the antenna is said to be circularly polarized. If none of the above exist, then the antenna is said to be elliptically polarized [29, p. 473]. From the data the antenna polarization is shown to be both linear and circular. For 10 GHz and 20 GHz the phase difference is very close to $0$ or $180$ degrees. For 30 GHz the voltage magnitudes are nearly equal, but the phase is not equal to $\frac{\pi}{2}$. See Table 9 for the magnitude and phase data.

Table 9: LPMSAA polarization data.

| $f_0$ | $\lvert\vec{E}_\theta\rvert$ | $\vec{E}_\theta$ phase | $\lvert\vec{E}_\phi\rvert$ | $\vec{E}_\phi$ phase | V difference | phase difference |
|---|---|---|---|---|---|---|
| (GHz) | (V) | (degrees) | (V) | (degrees) | (V) | (degrees) |
| 10 | 0.699 | -157 | 0.103 | -152 | 0.59 | -5.1 |
| 20 | 0.964 | -64 | 0.153 | 101 | 0.81 | -165 |
| 30 | 3.54 | -166 | 3.16 | 119 | 0.38 | -285 |
| 40 | 3.53 | 168 | 13.1 | -58 | -9.57 | 226 |

## 4.5 Summary

An engineered drawing was provided to memorialize the layout of the LPMSAA. The drawing can be visualized as a mask of the copper traces and patches on top of a Roger's Duroid laminate stack-up. The simulated $S11$ and far-field data were presented for the LPMSAA. The data clearly shows the pass and fail results for the hypothesis.

# 5 Conclusions

## 5.1 Summary of The Results

The LPMSAA sweep results show that the antenna fails to provide a $VSWR < 1.8$ for at least $80\%$ of the pass band of 8-40 GHz. In addition, it can be noted that the $Z_{in}$ had modest swings throughout the pass-band. The swings are believed to be caused by impedance mismatches between the patches and port one. However, the bandwidth of 22 GHz does seem reasonable. The $R_L$ does have a downward trend from 8-34 GHz which is somewhat encouraging. Therefore, the antenna is resonant, but not as strong as desired.

The $HPBW$ results were good and very close to the required 20 degrees. Technically, the $HPBW$ failed only for the 10 GHz elevation slices. The array gain performance was better than expected at 5.5 dBi. The directivity was also very high, and for the 30-40 GHz pass-bands the efficiency was 100 $\%$. It is hard to believe the antenna has this high of an efficiency. The co and cross polarization performance was straight-forward and the results seem sensible. The antenna polarization is shown to have characteristics of linear

polarization from 10-20 GHz. The data does not make a strong argument for the antenna to be circular or elliptically polarized at the higher frequencies. The antenna polarity seems to be logical and is consistent with the research performed. Overall, the array performed very much as expected, except for the s-parameter results. The far-field results were better than expected and are reasonable for such a wide-bandwidth fixture. The antenna has an exceptionally high gain, so the propagation of, or reception of, radar signals should be strong in the elevation planes.

## 5.2 Compare LPMSAA to a Pasternack Standard Gain Horn Antenna

The SSEL has horn antennas to cover the radar bands mentioned previously. Specifically, for the upper Ka band a Pasternack PE9850/2F-20 standard gain horn is used [30]. Since the LPMSAA has excellent gain and directivity in the 30-40 GHz pass-band a comparison can be made between the Pasternack horn antenna and the LPMSAA. For convenience, the primary parameters are listed in Table 10. The horn antenna has a 3.5 GHz wider bandwidth and a lower $VSWR$. The LPMSAA has a higher input impedance and $VSWR$ respectively. The horn antenna is better matched to a typical 50 Ohm transmission line. In addition, for far-field measurements, a high gain antenna is preferred to offset the free space path loss between the target and the reference antenna. Clearly, the horn antenna has a substantially higher gain and very reasonable narrow $HPBW$. The $HPBW$ of the LPMSAA is approximately 5 degrees narrower than the horn antenna. One of the potential advantages of the LPMSAA would be a single antenna that could cover the entire 8-40 GHz bandwidth and have one connector. The LPMSAA does have a larger physical size, but this is expected because the fixture has 33 elements. The LPMSAA could be used in place of the horn antenna, but some compromises would have to be made.

Table 10: Comparison between Pasternack Horn antenna and the LPMSAA primary parameters.

| Parmeters | Pasternack | LPMSAA |
|---|---|---|
| Frequency Range (GHz) | 26.5-40 | 30-40 |
| $Z_{in}(Ohms)$ | 50 | 75 |
| $VSWR$ | 1.25 | 1.75 |
| Nominal Gain (dBi) | 20 | 12 |
| $HPBW$ (degrees) | 18.3 | 13 |
| Dimensions, HxLxW (mm) | 1.01 x 1.38 x 3.72 | 60 x 219 x 2 |

## 5.3 Potential Issues

Some of the unrealistic results discussed above could be a result of settings in ADS, the limitations of the software, or simply the design could have some flaws. One noted issue is the stack-up. In the ADS settings for the stack-up (the copper material setting) for the ground plane was set to perfect electric conductor. This could possibly contribute to unrealistic performance data. However, it is unclear if changes in this setting would make much of a difference. One could simply re-run the simulation with a realistic copper setting, or create the antenna and have it professionally tested to verify it's performance.

Another potential issue could be the $d_m$ section length for the right hand side patches (high frequency side). It is highly possible, the patches were placed in the incorrect order. The patches should be connected from high frequency to low frequency (similar to the left hand side). This could be a problem for the high-frequency performance in the K and Ka bands. Since the transmission line is designed as a feed and also a filter the high frequency signals could be attenuated on the right hand side. As an example, the largest patch on the left hand side is 8 GHz and the transmission line is designed in even multiples of $\lambda/2$. The transmission line feeding the 8 GHz patch looks like a high impedance to the higher frequencies. Therefore the transmission line length plays a critical role in the overall performance of the array. This could be part of the cause of the huge swings in the $Z_{in}$, $R_L$, and $VSWR$. This problem could possibly be solved by using a CEM program that has reliable parametric sweeps. In addition, the left hand side could also experience

discrepancies in the $d_m$ length. The equations in chapter 2 should only be used as a guide to set up the initial design. Parametric sweeps from the CEM program should be used to finalize the transmission line length.

A few potential issues were also found during the high frequency sweep of 30-40 GHz. An error message was reported by ADS stating: "The global maximal mesh cell size is 1.01 mm, corresponding to a mesh density of 5 cells per wavelength. It is generally not possible to get an accurate result below 10 cells per wavelength". An increase of the mesh density is recommended up to at least 20 cells per wavelength. Even though the mesh density was set to 10, the wavelength was so small in comparison. Therefore, the software generated this warning message.

Another error message was: "The distance between the layout pins for port 1 is electrically large above 13.67 GHz, S-parameters may become unphysical". This warning message is a result of the 1.57 mm substrate thickness. This thick of a substrate is unexpectedly too thick for the software to complete a competent sweep with one port. To solve this problem ADS recommends that two ports be used to drive the antenna. Port one is to be connected to the main transmission line (as usual) and port two is to be connected to ground. Next, port one is to be referenced to ground through port two. The above suggestions should fix these two error messages and result in a better estimate into the antenna's parameters. It is further recommended to use these settings for the entire 8-40 GHz sweep.

## 5.4 Suggested Test Methods

Since the LPMSAA will not be fabricated, a discussion about testing the antenna seems logical. Should one fabricate such an antenna the following is suggested for complete analysis of the LPMSAA. The research hypothesis should be tested using laboratory quality test equipment, and an anechoic chamber. The laboratory equipment and anechoic chamber will have adequate frequency range, be designed for far-field measurements of antennas in the frequency range of 8-40 GHz as per the requirements stated in equation (36). The

anechoic chamber will have known reflections and losses in the same band. The known sources of error will be shown on the final report, and losses will be deducted from the measurement results. The LPMSAA will be tested in the anechoic chamber for return loss magnitude, phase and VSWR over bandwidth. The antenna will be placed under a passive test and be swept in 1 MHz steps from 8-40 GHz to determine the efficiency and gain over bandwidth. The electric and magnetic field 2 dimensional and 3 dimensional pattern data will be provided with a three to five degree resolution, and include the front to back ratio. Pictures of the test setup are to be provided and provide details for the results to be posted in chapter 4.

Once the data sets are received from the testing company the data sets will be compared to the CEM simulation data. Specific comparisons to be evaluated will be the electric and magnetic field 2 dimensional slices, 3 dimensional plots, return loss magnitude and $VSWR$ versus bandwidth.

The accuracy of the simulated data compared to the actual test results is unknown and difficult to quantify. CEM programs estimate Maxwell's equations with a mesh over the radiating surface, with predefined mesh density levels. Increased mesh density yields higher accuracy, but will take considerable more time to compute the final results. There is no way to qualitatively compute the accuracy of the simulated results without comparing the simulation data to the measured data. Inaccuracies are expected for the above parameters, but simulation data should be comparable to the measured results. The error sources such as cable insertion loss, path loss, reflections, and other sources of losses, gains, or multi-path in the anechoic chamber will either be calibrated out, or deducted from the raw measurements. For passive measurements the measurement plane will be moved from the measurement device to the antenna connector. An experienced measurement and test house will be able to estimate the known errors and levels of multi-path that are expected.

## 5.5 Recommendations for Future Work

It is encouraged that others try to use the layout created and design files to improve on this design. A CEM program that has a working parametric sweep function is highly recommended. It is further recommended to run the sweeps as one continuous 8-40 GHz sweep and to avoid broken up data sets. Many CEM programs offer co-simulation support. Co-simulation leverages the use of multiple servers to speed up the simulation process. For this application and such a wide bandwidth co-simulaiton is highly recommended. However, at a minimum a computer with an I-7 processor and at least 32 gigabits of RAM is recommended.

# Appendix A

The array primary parameters were calculated using Matlab. The following screen shots show the equations for elements 1-17 respectively. See Table 3 for the data output. For elements 18-33 the equations are similar.

```
%%%%% all calcs done in mm!!! %%%%%%%%%%%%%%%%
clc; clear;
c=3.0e11;    %mm/s
%%%%%%%%%%%%%%%%%%%%%%%%%%%%%%%%%%%%%%%%%%%555
f=17.463e9;
er=2.2;  %FR4 permittivity could be as high as 4.7
h=1.575;     %Rogers Duroid 5880
lambda=c/f;  % find the wavelength in mm/s
%%%%%%%%%%%%%%%%%%%%%%%%%%%%%%%%%%%%%%%%%%%%%%
L1=c/(2*f*sqrt(er));
W1=L1;
%find the e effective,
eeff=((er+1)/2)+((er-1)/2)*(1/(sqrt(1+12*h/W1)));

%%%%%%%%%%%%%%%%%%%%%%%% Equation #2 from mlpa using ckt sim.. %%%%%%%%%%%%%%%
%%%%%%%%%%%%%%%%% determine the fringing effect of the patch %%%%%%%%%%%%%%%
delta_L=0.412*h*(((eeff+0.3)*(W1/h + 0.264)))./(((eeff-0.258)*(W1/h + 0.8)));
%Below is the actual length required for f0, with fringing effect removed
L_actual=c/(2*f*sqrt(eeff))-2*delta_L;   %Equation #14-7 from Balanis
L1=L_actual;
W1=L1;
% find the actual starting frequency with the new patch length
f0=c/((2*(L1+2*delta_L))*sqrt(eeff));  %Equation #1 from mlpa..
```

Figure 52: Initial $W$, $L$ calculations.

```
lambda0=c/f0;  % this is the new resonant wavelength due to fringing effects
%%%%%%%%%%%%%%%%%%%%%%%% find lambda g length  %%%%%%%%%%%%%%%%%%%%%%%%%%%%%
lambda_g=lambda0/sqrt(eeff);
half_wave=lambda_g/2;
%%%%%%%%%%%%%%%%%%%%%%%%%%%%%%%%%%%%%%%%%%%%%%%%%%%%%%%%%%%%%%%%%%%%%%%%%%%%
%%%%%%%%%%%%%%%% wavelenght ratio, see Balanis Fig 14.10 %%%%%%%%%%%%%%%%%%%
slot_width_to_lambda0=W1/lambda0;  % determine the ratio of slot width to
%%%%%%%%%%%%%%%%%%%%%% find Inset depth of feed %%%%%%%%%%%%%%%%%%%%%%%%%%%%
%determine the free space wavelength
k0=2*pi./lambda0;     %determine the free space wave
%%%%%%%%%%%%%%%%%%%%%%%%%%%%%%%%%%%%%%%%%%%%%%%%%%%%%%%%%%%%%%%%%%%%%%%%%%%%
%%%%%%%%%%%%%%%%%%%%%%%%%%%% Integrate teh G12 fnc%%%%%%%%%%%%%%%%%%%%%%%%%%
fun=@(x,k0,W1,L1) ((((sin((k0.*W1./2).*cos(x))./cos(x)).^2).
*(besselj(0,k0*L1.*sin(x))).*((sin(x)).^3));
G12=(1./(120*(pi^2)))*(integral(@(x)fun(x,k0,W1,L1),0,pi));
%compute the integral of G12 from 0-pi
%%%%%%%%%%%%%%%%%%%%%%%%%%%% Integrate the G1 function %%%%%%%%%%%%%%%%%%%%%
%%%%%%%%%%%%%%%%%%%%%%%%%%%%%%%%%%%%%%%%%%%%%%%%%%%%%%%%%%%%%%%%%%%%%%%%%%%%
fun=@(x,k0,W1,L1) ((((sin((k0.*W1./2).*cos(x))./cos(x)).^2)).*((sin(x)).^3);
I1=(integral(@(x)fun(x,k0,W1,L1),0,pi)); %compute the integral of G12 from 0-pi
G1=I1/(120*(pi^2));
%%%%%%%%%%%%%%%%%%%%%%%%%%%%%%%%%%%%%%%%%%%%%%%%%%%%%%%%%%%%%%%%%%%%%%%%%%%%
```

Figure 53: Conductance equations.

```
%%%%%%%%%%%%%%%%%%%%%%%%%%%% compute Rin %%%%%%%%%%%%%%%%%%%%%%%%%%%%%%%%%%%
%%%%%%%%%%%try to evaluate I1 and then calc G1 using the soln in Balanis book
Rin=1./(2*(G12+G1));
%%%%%%%%%%%%%%%%%%%%%%%%%%%%%%%%%%%%%%%%%%%%%%%%%%%%%%%%%%%%%%%%%%%%%%%%%%%%
%%%%%%%%%%%%%%%%%%%%%%%%%%%% Find inset depth for Rin =100 Ohms%%%%%%%%%%%%%%
y=acos(sqrt(100/Rin));
y0=y*L1/pi;   %%%%%%%%%%%%%%%% y0 is the inset depth
%%%%%%%%%%%%%%%%%%%%%%%%%%%%%%%%%%%%%%%%%%%%%%%%%%%%%%%%%%%%%%%%%%%%%%%%%%%%
%%%%%%%%%%%%%%%%%%%%%%%%%%%% Set W0, width of inset feed 3mm
W0=1.5;
%%%%%%%%%%%%%%%%%%%%%%%%%%%%%%%%%%%%%%%%%%%%%%%%%%%%%%%%%%%%%%%%%%%%%%%%%%%%
%%%%%%%%%%%%%%%%%%%%%%%%%%%% Find Zc, this eqn assumes W0/h >1,
%%%%%% for our case W0/h=3/1.6 ~1.875
Zc=(120*pi/sqrt(eeff))*1./(W0/h+1.393+0.667*log(W0/h+1.44));
%%%%%%%%%%%%%%%%%%%%%%%%%%%%%%%%%%%%%%%%%%%%%%%%%%%%%%%%%%%%%%%%%%%%%%%%%%%%
% calculate all the frequencies
tao=1.05; % multiplying factor alternativ
m=17;        % number of elements in antenna
%%%%%%%%%%%%%%%%%%%%%%%%%%%%%%%%%%%%%%%%%%%%%%%%%%%%%%%%%%%%%%%%%%%%%%%%%%%%
```

Figure 54: $R_{in}$ and $Z_0$ equations.

```
%%%%%%%%%%%%%%%%%%%%%%%%%%%%%%%%%%%%%%%%%%%%%%%%%%%%%%%%%%%%%%%%%%%%%%%%%%%%
% Im from Conf Paper, "The Design of 9 Element Quasi u-strip lp Ant"
Im=6.59;  % Im feed length
L2=W1-y0;   %inset depth
S11=0.5;    % set S1 and S2 gap at 0.5mm, S1=S2=0.5mm
W22=1.5;    %the feed line width is consistent at 1.5mm
Gap=2*S11+W22;  %determine the residual ears of MACLin3 for W1 and W3
W11=(W1-Gap)/2; %the overall width of patch less the
                %gap/2 are Maclin3 W1 and W3
%%%%%%%%%%%%%%%%%%%%%%%%%%%%%%%%%%%%%%%%%%%%%%%%%%%%%%%%%%%%%%%%%%%%%%%%%%%%
% Find dm length for each patch,
% which should be an integer multiple of 0.5xlambda_g
l1=39;      %needed for patches 17-1
l2=39.2;    %needed for patches 18-34
dm=0;
tee=1.5;     %tee junction for dm to Im's
curve=4.7;
dm_margin=0;    % 5mm margin for each dm feed
patch_l=tee+Im+y0+l1+dm_margin;
x=1;
x5wave=half_wave;
```

Figure 55: Main transmission line equations.

```
while x5wave<patch_l
        x=x+1;
        x5wave=half_wave*x;
        dm=x5wave-(patch_l-dm_margin);
  end
ehwl=patch_l+dm-dm_margin;    %the entire half wavelength for this patch
elofxmissionline=dm+l1+tee;
%%%%%%%%%%%%%%%%%%%%%%%%%%%%%%%%%%%%%%%%%%%%%%%%%%%%%%%%%%%%%%%%%%%%%%%%%%%%
fprintf('\n');
fprintf('****Begin Array Scaling Calcs *********');fprintf('\n');
fprintf('******* Start with patch 17 *************');fprintf('\n');
patch_num=18;
for n=1:m
    format shorte;
    patch_num=patch_num-1;

    fprintf('****************************************'); fprintf('\n');
    fprintf('Patch # %3d',patch_num);fprintf('\n');
    fprintf('frequency= %3e, dm=%f, Ant Width=%3f, MLOC L=%3f',
    f0,dm,W1,L2);fprintf('\n');
    fprintf('\n');
    fprintf('W1 & W3=%3f, S1 & S2=%f, W2=%f,y0=%3f,Im=%3f',
    W11,S11,W22,y0,Im);fprintf('\n');
    fprintf('\n');
    fprintf('lambda_g=%3f, 1/2 lambda_g=%3f, half wave multiplier=%3d,
    entire half wave length=%3f,eeff=%f',lambda_g,half_wave,x,ehwl ,eeff)
```

Figure 56: Array scaling equations.

```
    fprintf('length of trans line vertical=%3f',elofxmissionline)
    ;fprintf('\n');
    fprintf('\n');
    fprintf('************************************************************');
    %%%%%%%%%%%%%%%%%%%%%%%%%%%%%%%%%%%%%%%%%%%%%%%%%%%%%%%%%%%%%%%%
    previous_feed=ehwl-y0-Im;  % need to add in the previous feed.
    f0=f0/tao;
    W1=W1*tao;
    L1=W1;
    Im=Im*tao;
lambda=c/f0;  % find the wavelength in mm/s
%%%%%%%%%%%%%%%%%%%%%%%%%%%%%%%%%%%%%%%%%%%%%%%%%%%%%%%%%%%%%%%%
L1=c/(2*f0*sqrt(er));
% %%%%%%%%%%%%%%%%%%%%%%%%%%%Equation #3 from mlpa using ckt sim
eeff=((er+1)/2)+((er-1)/2)*(1/(sqrt(1+12*h/W1)));
%%%%%%%%%%%%%%%%%%%%%%%%% Equation #2 from mlpa using ckt sim.. %%%%%%%%%%%
%%%%%%%%%%%%%%%%% determine the fringing effect of the patch %%%%%%%%%%%%%%
delta_L=0.412*h*(((eeff+0.3)*(W1/h + 0.264)))./(((eeff-0.258)*
(W1/h + 0.8)));
%Below is the actual length required for f0, with fringing effect removed
%%%%% calculated in mm
L_actual=c/(2*f0*sqrt(eeff))-2*delta_L;   %Equation #14-7 from Balanis
L1=L_actual;
W1=L1;
```

Figure 57: Fringing effect equations.

```
% find the actual starting frequency with the new patch length
%%actual frequency with delta_L in calculation,
%c in mm/s, L in mm, delta_L in mm,
f0=c/((2*(L1+2*delta_L))*sqrt(eeff));  %Equation #1 from mlpa..
%%%%%%%%%%%%%%%%%%%%%%%% find dm length  %%%%%%%%%%%%%%%%%%%%%%%%%%%%%
    lambda0=c/f0;
    lambda_g=lambda0/sqrt(eeff);
    half_wave=lambda_g/2;
    %%%%%%%%%%%%%%%%%%%% find Inset depth of feed %%%%%%%%%%%%%%%%%%%%%%
    %determine the free space wavelength
    k0=2*pi./lambda0;     %determine the free space wave
    %%%%%%%%%%%%%%%%%%%%%%%%%%%% Integrate the G12 fnc%%%%%%%%%%%%%%%%%%
    fun=@(x,k0,W1,L1) ((((sin((k0.*W1./2).*cos(x))./cos(x)).^2).
    *(besselj(0,k0*L1.*sin(x))).*((sin(x)).^3));
    G12=(1./(120*(pi^2)))*(integral(@(x)fun(x,k0,W1,L1),0,pi));
    %compute the integral of G12 from 0-pi
    %%%%%%%%%%%%%%%%%%%%%%%%%%%% Integrate the G1 function %%%%%%%%%%%%%%
    fun=@(x,k0,W1,L1) ((((sin((k0.*W1./2).*cos(x))./cos(x)).^2)).
    *((sin(x)).^3);
    I1=(integral(@(x)fun(x,k0,W1,L1),0,pi)); %compute the integral of
    %G12 from 0-pi
    G1=I1/(120*(pi^2));
    Rin=1./(2*(G12+G1));
```

Figure 58: Starting frequency and $R_{in}$ equations.

```
    %%%%%%%%%%%%%%%%%%%%%%%%%%% Find inset depth for Rin =100 Ohms%%%%%%%
    y=acos(sqrt(100/Rin));
    y0=y*L1/pi;    %%%%%%%%%%%%%%%% y0 is the inset depth
    L2=W1-y0;
    W11=W11*tao;
    W11=(W1-Gap)/2;
    MLIN_L=Im-y0;
    %%%%%%%%%%%%%%%%%%%%%%%%%%%%%%%%%%%%%%%%%%%%%%%%%%%%%%%%%%%%%%%%%%%%%%%
% Find dm length for each patch, which should be an integer multiple
of 0.5xlambda_g
dm_margin=3;
tee=1.5;     %tee junction for dm to Im's
if patch_num == 1   %must have the double = sign??
            tee=curve;
end
patch_next=previous_feed+tee+Im+y0+dm_margin;

x=1;
x5wave=half_wave;
while x5wave<patch_next
        x=x+1;
        x5wave=half_wave*x;
end
dm=x5wave-(patch_next-dm_margin);
ehwl=patch_next+dm-dm_margin;
%the entire half wavelength for this patch
elofxmissionline=previous_feed+dm+tee;
end
```

Figure 59: $d_m$ and main transmission line equations.

# Appendix B

The following screen shots are provided to assist any future researcher in the use of ADS. In ADS one needs to create a schematic with the TLines-Microstrip parts as in Figure 60. Next, the dimensions of each part will make up the patches and transmission lines as in Figure 61.

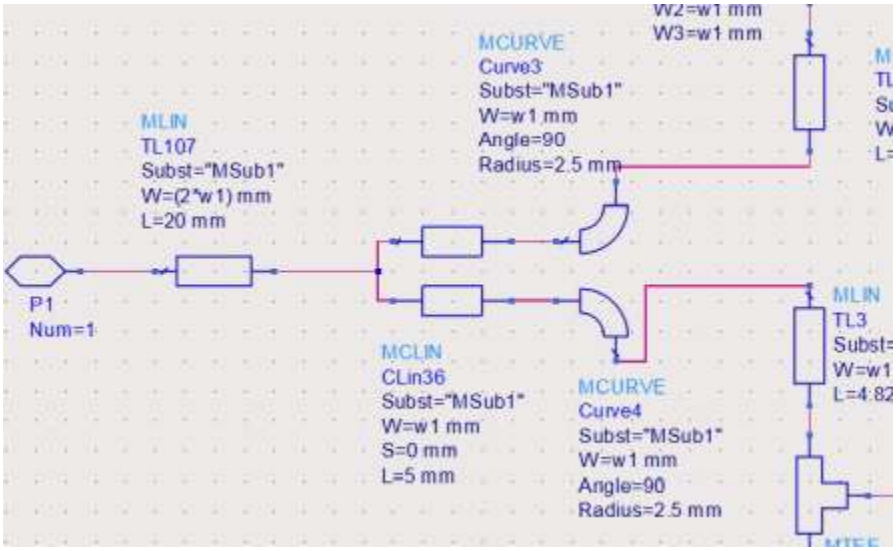


Figure 60: ADS screen shot of 50 Ohm feed transmission line.

When the schematic is complete it is next converted into a layout as in Figure 62. Following the layout creation the emSetup is completed to create the stack up, frequency sweeps, port settings, and mesh settings as in Figures 63, 64, 65, and 66. Finally, the EM sweeps can be started.

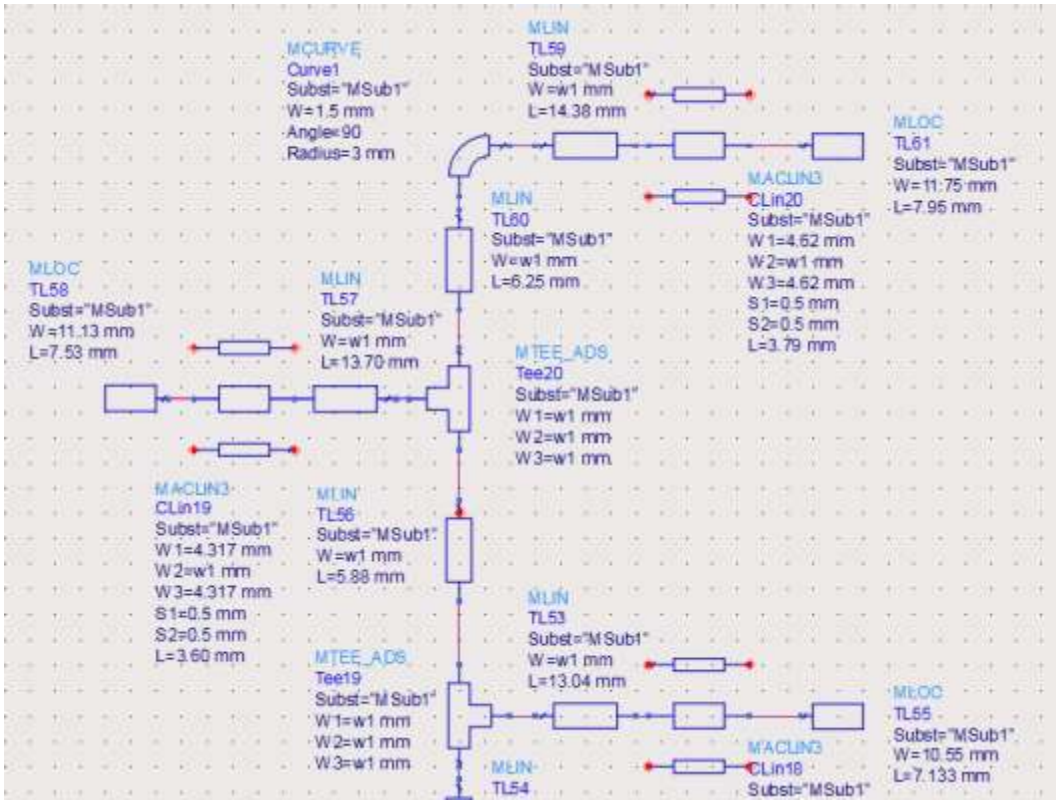


Figure 61: ADS screen shot 8 and 8.4 GHz patches.

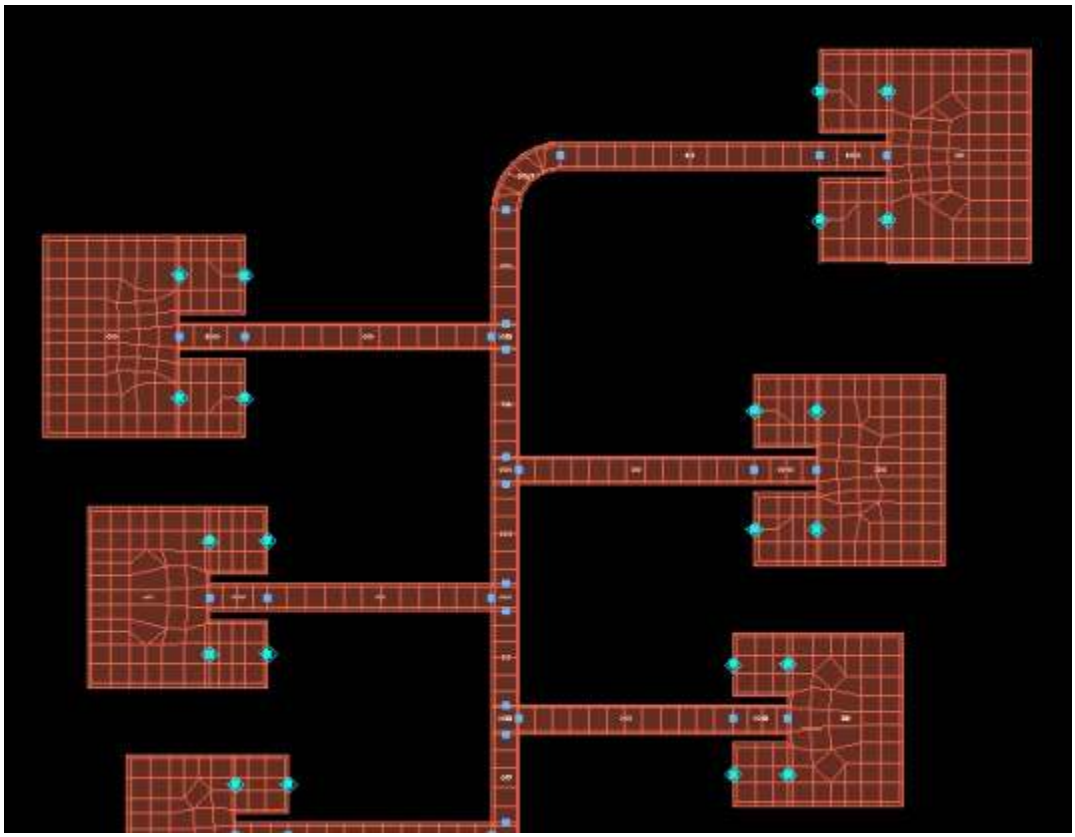

Figure 62: ADS screen shot 8 and 8.4 GHz patches in layout view.


Figure 63: ADS screen shot of stack up.


Figure 64: ADS screen shot of frequency sweep setup window.

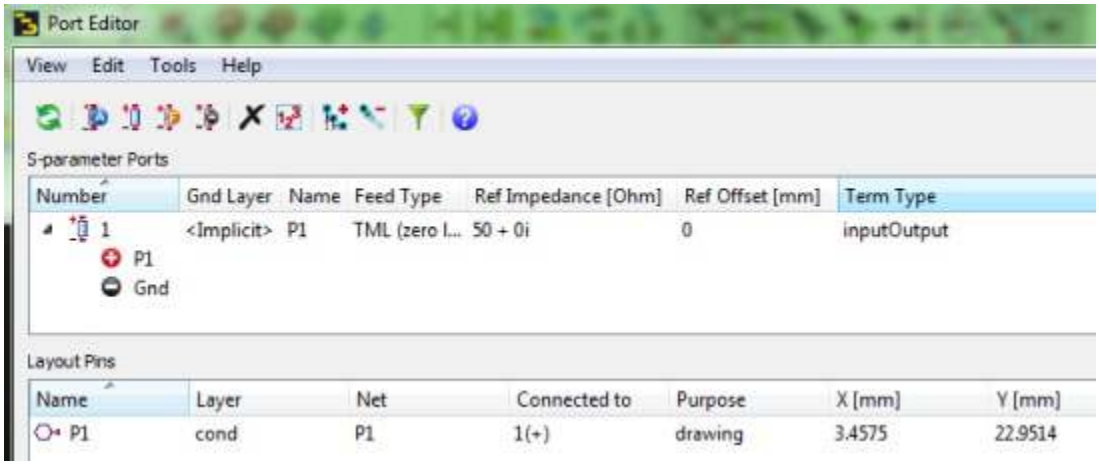


Figure 65: ADS screen shot of port settings.

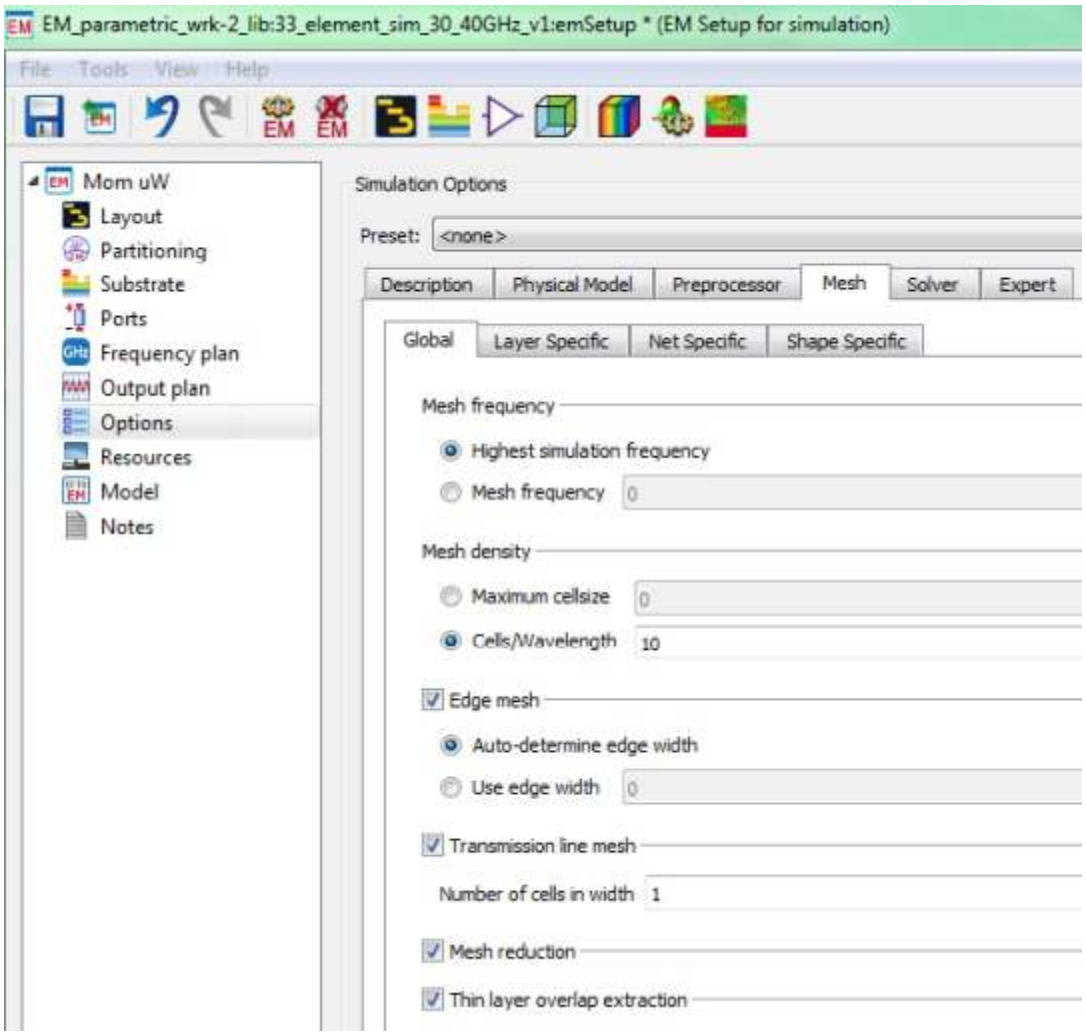


Figure 66: ADS screen shot of mesh settings.

# REFERENCES


[1] E. Shepherd, C. Rockett, T. Almutairi, E. Sum, J. Compaleo, and M. Saville, "Small antenna positioning system design at wright state university," 07 2015, pp. 1442–1443.

[2] K. R. Girish Kumar, *Broadband Microstrip Antennas*. Artech House antennas and propagation library, 2003, ch. 1, p. 11.

[3] R. Munson, "Conformal microstrip antennas and microstrip phased arrays," *IEEE Trans Antennas Propagation*, pp. 74–78, Jan 1974.

[4] C. A. Balanis, *Antenna Theory Analysis and Design, Third Edition*. Wiley, 2014.

[5] W. Stutzman and G. Thiele, *Antenna Theory and Design*, ser. Antenna Theory and Design. Wiley, 2012.

[6] M. K. A. Rahim, M. N. A. Karim, T. Masri, and A. Asrokin, "Comparison between straight and u shape of ultra wide band microstrip antenna using log periodic technique," in *2007 IEEE International Conference on Ultra-Wideband*, Sept 2007, pp. 696–699.

[7] G. Bozdag and A. Kustepeli, "Subsectional tapered fed printed lpda antenna with a feeding point patch," *IEEE Antennas and Wireless Propagation Letters*, vol. 15, pp. 437–440, 2016.

[8] K. C. Lin and Y. C. Lin, "Printed log-periodic antenna fed by uwb balun for multi-polarization operation," in *2013 IEEE Antennas and Propagation Society International Symposium, APSURSI*, July 2013, pp. 1306–1307.

[9] P. S. Hall, "Multioctave bandwidth log-periodic microstrip antenna array," *IEEE Proceedings H - Microwaves, Antennas and Propagation*, vol. 133, no. 2, pp. 127–136, April 1986.

[10] R. DuHamel and D. Isbell, "Broadband logarithmically periodic antenna structures," in *1958 IRE International Convention Record*, vol. 5, March 1957, pp. 119–128.

[11] M. K. A. Rahim and P. Gardner, "Microstrip log periodic antenna using circuit simulator," in *Antennas, Propagation and EM Theory, 2003. Proceedings 2003 6th International Symposium on*, 2003, pp. 202–205.

[12] M. I. Nawaz, H. Zhao, M. Nawaz, K. Zakim, S. Zamin, and A. Khan, "A review on wideband microstrip patch antenna design techniques," 08 2013, pp. 1–8.

[13] A. Amini, H. Oraizi, and M. A. C. zadeh, "Miniaturized uwb log-periodic square fractal antenna," *IEEE Antennas and Wireless Propagation Letters*, vol. 14, pp. 1322–1325, 2015.

[14] M. Dadel and S. Srivastava, "Arrays of patch antenna using log periodic property," 12 2011.

[15] M. I. Nawaz, H. Zhao, M. Nawaz, K. Zakim, S. Zamin, and A. Khan, "A review on wideband microstrip patch antenna design techniques," 08 2013, pp. 1–8.

[16] D. Pozar, *Microwave Engineering, 4th Edition*. Wiley, 2011.

[17] D. Pozar, "Microstrip antennas," *Proceedings of the IEEE*, vol. 80, pp. 79–91, 01 1992.

[18] R. Munson, "Truncated rectangular microstrip antenna with h and u slot for broadband," *International Journal of Engineering Science and Technology (IJEST)*, pp. 114–118, Jan 2013.

[19] D. Y. Zhuang, "EE-6460 microwave engineering II," 2013.

[20] (2011-2016) Antenna theory website. [Online]. Available: http://www.antenna-theory.com/antennas/patches/antenna.php

[21] M. Rahim and P. Gardner, "The design of nine element quasi microstrip log periodic antenna," 11 2004, pp. 132 – 135.

[22] H. Pues, lr., J. Bogaers, lr., R. Pieck, lr., A. V. de Capelle, and D. lr., "Wideband quasi-log-periodic microstrip antenna," *Proceedings of the IEEE*, vol. 128, no. 3, pp. 159–163, 1981.

[23] (2011-2016) Antenna theory website. [Online]. Available: http://www.antenna-theory.com/basics/fieldRegions.php

[24] (2011-2016) Antenna theory website. [Online]. Available: http://www.antenna-theory.com/basics/gain.php

[25] "IEEE Standard for Definitions of Terms for Antennas," *IEEE Transactions on Antennas and Propagation*, vol. 17, no. 3, pp. 262–269, May 1969.

[26] I. Bahl and D. Trivedi, "A designer's guide to microstrip line," *Microwaves*, vol. 16, pp. 174–176, 178, 180, 182, 05 1977.

[27] P. I. Thomas Rylander, Anders Bondeson, *Computational Electromagnetics, second edition*. Springer, 2013.

[28] P. Pino, "Intermateabillity of sma, 3.5 and 2.92 mm connectors," *Microwave Journal Cables and Connectors Supplement*, 2007.

[29] Keysight, *Electromagnetic*, 2019.

[30] (2017) Pasternack pe9850/2f-20. [Online]. Available: https://www.pasternack.com/standard-gain-horn-waveguide-size-wr28-20-db-gain-292mm-female-pe98502f-20-p.aspx